CHALMERS
UNIVERSITY OF TECHNOLOGY

Impedance measurement techniques for DC-biased systems

Literature study and experimental evaluation of interfaces for impedance measurement of DC-biased systems in electric vehicles.

Degree project report in Mobility Engineering

AXEL HENRIKSSON

DEPARTMENT OF ELECTRICAL ENGINEERING

CHALMERS UNIVERSITY OF TECHNOLOGY
Gothenburg, Sweden 2025
www.chalmers.se

Degree project report 2025

Impedance Measurement Techniques for DC-biased Systems

Literature study and experimental evaluation of interfaces for impedance measurement of DC-biased systems in electric vehicles.

AXEL HENRIKSSON

CHALMERS
UNIVERSITY OF TECHNOLOGY

Department of Electrical Engineering
Chalmers University of Technology
Gothenburg, Sweden 2025

Impedance measurement techniques for DC biased systems
Literature study and experimental evaluation of interfaces for impedance measurement of DC-biased systems in electric vehicles.
AXEL HENRIKSSON

Supervisor: Divyaraj Gadhavi & Anders Lasson, Volvo Cars Corporation
Examiner: Torbjörn Thiringer, Department of Electrical Engineering

Degree project report 2025
Department of Electrical Engineering
Chalmers University of Technology
SE-412 96 Gothenburg
Sweden
Telephone +46 31 772 1000

Typeset in LaTeX
Gothenburg, Sweden 2025

Impedance measurement techniques for DC biased systems
Literature study and experimental evaluation of interfaces for impedance measurement of DC-biased systems in electric vehicles.
Axel Henriksson
Department of Electrical Engineering
Chalmers University of Technology

Abstract

This thesis compiles information about six methods for impedance measurement of DC biased systems. It describes a physical interface for low-voltage Devices Under Test (DUTs) using the shunt-through method with DC-blocking capacitors. The interface is used to measure impedance versus frequency of three pouch cells of different dimensions and chemistries.

In addition to the cell measurements, a separate set of measurements are carried out on inductors and capacitors with and without the use of the DC-blocking interface.

The measurements show how parameters such as heat, conductor length and measurement setup affect the measured impedance. An interface model is presented that explains in what frequency and DUT impedance ranges each parasitic interface parameter affects the measurement results, and in what way.

The conclusion of the thesis is that the used capacitor-based impedance measurement method was not accurate when measuring the low impedance of an electric vehicle battery cell. However, with the modification and improvements outlined in the thesis, the interface type could be used to measure devices with larger impedance, such as a complete high voltage electric vehicle battery consisting of the same cells.

Keywords: EMC, Batteries, impedance, EIS, Impedance Spectroscopy, Power Electronics.

Acknowledgements

I would like to thank my supervisors at VCC; Anders Lasson and Divyaraj Gadhavi for the trust they have put in me, for the opportunity to write a thesis about an interesting subject, and for their guidance and support through the whole project.

Secondly, I would like to thank my examiner Torbjörn Thiringer for taking time out of his schedule to not only take on the role as examiner, but also for going beyond, helping in the provision of equipment, sources and expertise.

Thirdly, I would like to thank Raik Orbay for showing great interest in the thesis, providing new perspectives, discussing ideas and working on finite element models, the results of which unfortunately were not ready in time for this report.

Lastly, I would like to thank the other thesis workers and supervisors at the department for making my time at Volvo all the more enjoyable.

Axel Henriksson, Gothenburg, April 2025

List of Acronyms

AC	Alternating Current
BMS	Battery Management System
CM	Common Mode
CMC	Common Mode Choke
CMRR	Common Mode Rejection Ratio
DC	Direct Current
DM	Differential Mode
DUT	Device Under Test
EIS	Electrochemical Impedance Spectroscopy
ESL	Equivalent Series Inductance
ESR	Equivalent Series Resistance
FRA	Frequency Response Analyzer
HV	High Voltage
IC	Integrated Circuit
IA	Impedance Analyzer
LISN	Line Impedance Stabilization Network
LV	Low Voltage
ML	Multi-Layered
MLCC	Multi-Layered Ceramic Capacitor
NC	Normally Closed
NO	Normally Open
OTS	Off The Shelf
PSRR	Powe Supply Rejection Ratio
SNR	Signal To Noise Ratio
SMT	Surface Mount
SUT	System Under Test
VNA	Vector Network Analyzer
VCC	Volvo Cars Corporation

Contents

1
Introduction

1.1 Background

With electrification of transport being considered one of the pillars of the green transition, the demand for electric vehicles (EV) and electric vehicle research has increased drastically.

For EV manufacturers the focus is on increasing product value while simultaneously reducing development and manufacturing cost. In order to improve and optimize existing EV high voltage (HV) systems, increasingly detailed and accurate knowledge of the system behaviour is required.

For departments responsible for the products' adherence to electromagnetic compatibility (EMC) directives, accurate knowledge of their subsystems' intended as well as unintended electrical behaviour is vital. Knowledge of the subsystems' impedance from DC up to GHz allows for effective design of filters that reduce the system's electromagnetic emissions and thus improve electromagnetic (EM) compliance. This system knowledge also opens up for new design optimizations, leading to improved performance and reliability per cost.

Due to the high sensitivity to component geometry and synergy, measurements of these impedances are ideally carried out on the complete powertrain as it is to be used for the application. This poses a challenge as off-the-shelf (OTS) impedance measurement instruments are incompatible with the high voltages of the powertrain.

1.2 Previous work

Volvo Cars and Chalmers have previously collaborated on creating time- and frequency-domain models of electric powertrains. The project presented in [1] models the complete powertrain of a Volvo Car. For this purpose EIS measurements were conducted on single cells, a small number of active cells, and on the complete battery after the cells of the pack had been discharged and made inert. The results were compared with pre-existing full battery impedance data and it was found that extrapolating single cell behaviour to the complete pack level fails to approximate the true pack impedance above 2 kHz. At high frequencies, the inductive effects of conductors and other components will dominate the pack level impedance. It was also found that inert packs are not entirely representative of the energized pack. The report presents

a detailed impedance model of the battery pack capturing both Differential-Mode (DM) and Common-Mode (CM) behaviour over a wide frequency range[1].

Per Widek conducted high-frequency, battery pack level impedance measurements with the help of a capacitive DC blocking interface in his licentiate thesis[2]. The approximate bandwidth was 600 Hz to 1 MHz. Measurements were conducted on a 750 VDC system. Information on the specifics of the measurement interface is restricted.

Reference [3] presents a method of measuring frequency-dependent impedance of high-voltage batteries. Few specifics are provided and the measurement accuracy is not thoroughly discussed.

In the literature there is a lack of documented impedance measurement methods that can measure impedance of DUTs with a DC-bias of up to 800 V.

1.3 Purpose

The purpose of this thesis is to lay the foundation for the development of an impedance measurement method that is applicable for energized HV EV batteries and powertrains. The end goal of the method is to enable the collection of impedance data used in guiding the design process of EMC filters for any measured system.

The thesis will achieve this goal by investigating what is required to go beyond the limited voltage and frequency range of documented impedance measurement methods. This will be done through literature review, construction and validation of an exemplary low voltage interface; and through a proposal for an interface capable of HV battery impedance measurement. The goal of the proposed method is to enable measurements up to 50 MHz at the presence of DC voltages of up to 800 VDC. Both common mode and differential mode measurements are to be investigated.

The thesis intends to identify the possible limitations, compromises and sources of error that need to be regarded in the design of these kinds of interfaces. It also proposes ways for future interfaces to further improve the measurement bandwidth.

2
Theory

2.1 Impedance

Impedance is the complex relation between AC voltage and current. The impedance of an electric circuit element determines the phase shift and amplitude ratio between the complex voltage across the element and the complex current through it;

$$\bar{Z} = R + jX = \frac{\bar{V}}{\bar{I}} \tag{2.1}$$

where $R = \mathrm{Re}(\bar{Z})$ is the element's resistance, and $X = \mathrm{Im}(\bar{Z})$ its reactance. Thus, for a purely resistive element, the impedance is only real;

$$\bar{Z}_{\mathrm{R}} = R \tag{2.2}$$

For capacitive and inductive elements the reactance varies by frequency. As;

$$\bar{Z}_{\mathrm{C}} = jX_C = \frac{1}{j\omega C} \tag{2.3}$$

$$\bar{Z}_{\mathrm{L}} = jX_L = j\omega L \tag{2.4}$$

where L is element inductance, C is element capacitance and $\omega = 2\pi f$ is the angular frequency of the AC voltage or current.

2.1.1 Representation

Impedance can be represented in different ways that are presented in this section. A simple impedance network is used as an example (Figure 2.1) and consists of $C = 1\,\mu\mathrm{F}$, $L = 1\,\mathrm{mH}$ and $R = 1\,\mathrm{k\Omega}$ connected in series.

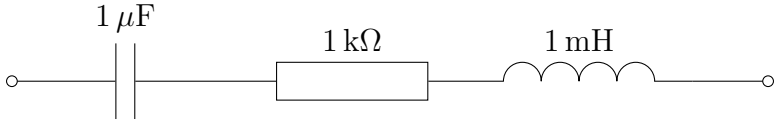

Figure 2.1: Example circuit model.

Its impedance $\bar{Z}$ can be expressed analytically using $j\omega$ as

$$\bar{Z} = \frac{1}{j\omega C} + R + j\omega L \tag{2.5}$$

or

$$\bar{Z} = R + j\left(\omega L - \frac{1}{\omega C}\right) \tag{2.6}$$

This results in an impedance magnitude of

$$\left|\bar{Z}\right| = \sqrt{R^2 + \left(\omega L - \frac{1}{\omega C}\right)^2} \tag{2.7}$$

and an impedance phase of

$$\arg \bar{Z} = \arctan\left(\frac{\omega L - \frac{1}{\omega C}}{R}\right) \tag{2.8}$$

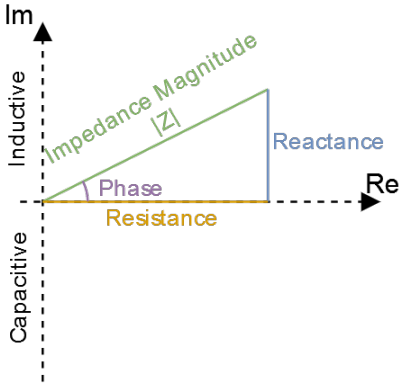

(a) Cartesian representation of impedance at a specific frequency.

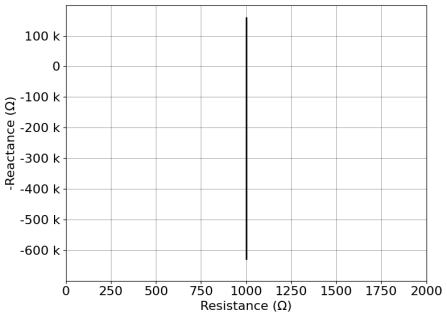

(b) Nyquist representation from 1 Hz to 50 Mhz of the impedance of the circuit in Figure 2.1.

Figure 2.2: Representations of the impedance of the circuit in Figure 2.1.

From the expressions in section 2.1, the impedance can be presented as in Figure 2.2a. For non-ideal elements, this only represents the DUT impedance at a specific frequency.

As the impedance of real components vary with frequency, impedance is often represented in a nyquist-plot such as the one seen in Figure 2.2b. Here, the DUT resistance and reactance are plotted on the x- and y-axis respectively. This representation is commonly used in Electrochemical Impedance Spectroscopy (EIS) to make the relation between physical phenomena and cell impedance more intuitive.

For battery cell EIS data, the convention is to invert the imaginary axis so that negative (capacitive) reactance is positive (up) and positive (inductive) reactance is negative (down). This convention is followed in Figure 2.2b and all following nyquist-plots.

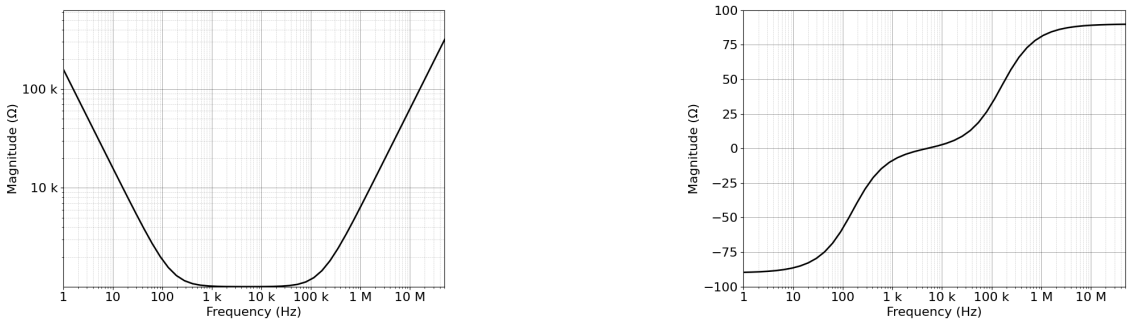

(a) Impedance magnitude.

(b) Impedance phase.

Figure 2.3: Impedance of the example circuit in Figure 2.1.

.

By separating impedance magnitude and phase, the frequency dependent impedance can be represented in a Bode diagram (Figure 2.3). In this representation each element can be seen to dominate in its own frequency band. The DUT can be considered capacitive up to 300 Hz, resistive between 300 Hz and 100 kHz, and inductive above 100 kHz. This is seen both in the slope of the impedance magnitude plot (Figure 2.3a), and in the phase of the DUT impedance (Figure 2.3b). A decreasing slope for the impedance magnitude and a phase of $-90\,^\circ$ indicates capacitive behaviour; no impedance slope and a phase of $0\,^\circ$ indicates resistive behaviour; a decreasing impedance slope and a phase of $90\,^\circ$ indicates inductive behaviour.

2.1.2 Capacitance

Capacitance is the ability of two conductive elements, that are electrically isolated but still capacitively coupled, to store electric charge.

Theoretically, the capacitance between two plates can be calculated as

$$C = \frac{\epsilon A}{d} \tag{2.9}$$

where ϵ is the dielectric absolute permittivity, A is the area with which the plates overlap, and d is the distance between the plates.

Fringe capacitance is additional capacitance that extends outside the area with which the plates overlap.

2.1.3 Inductance

Inductance is the tendency of a conductor to resist change in the current conducted in it (see (2.10)).

$$v(t) = L\frac{di}{dt} \tag{2.10}$$

A change in this current changes the magnetic flux surrounding the conductor. The inductance of a conductor increases when it is ”easier” to change this electric field.

For example, a conductor surrounded by a toroid of a material with low reluctance (i.e. high permittivity) has a higher inductance than one surrounded only by air.

2.1.3.1 Circuit loop area

The area which an electrical conduction path forms in space affects the leakage inductance of the conductor. A large loop area results in higher leakage inductance according to [4];

$$L_{\text{loop}} \approx \mu_0 \mu_{\text{r}} \left(\frac{D}{2}\right) \cdot \left[\ln\left(\frac{8 \cdot D}{d}\right) - 2\right]. \tag{2.11}$$

A large loop area also makes the circuit in question sensitive to external electromagnetic flux interacting with the loop area. This flux may induce small undesirable currents, i.e. disturbances, in the circuit.

2.1.4 Non-electrical elements

In some cases, non-linear elements that have no electrical equivalent are used for phenomena which cannot otherwise be expressed. One example is the Warburg impedance shown below;

$$\bar{Z}_{\text{W}} = \frac{\sigma}{\sqrt{\omega}} - j\frac{\sigma}{\sqrt{\omega}} \tag{2.12}$$

$$\sigma = \frac{RT}{Az^2F^2\sqrt{2}} \left(\frac{1}{\sqrt{D_{\text{o}}}c_{\text{o}}^{\text{b}}} + \frac{1}{\sqrt{D_{\text{R}}}c_{\text{R}}^{\text{b}}}\right) \tag{2.13}$$

For cell modelling, the Warburg impedance is often used to achieve a constant impedance phase below a certain frequency. This behaviour is for modelling chemical phenomena [5] and is irrelevant for measurements above 1 kHz.

2.1.5 Measurement

The impedance of a component is measured by either applying a voltage across it and measuring the resulting current (potentiostatic measurement), or injecting a current into it and measuring the resulting voltage (galvanostatic measurement). This is usually done across a specific frequency range for passive components, filters and antennas.

Dedicated impedance measurement instruments such as vector network analyzers (VNAs), Impedance Analyzers (IAs) and Frequency Response Analyzers (FRAs) combine both excitation and measurement in a simple package.

Other instruments are specifically designed for Electrical Impedance Spectroscopy (EIS) where there often is a DC bias present. An example is potentiostats from Gamry Instruments, such as the Gamry Reference 3000.

2.1.6 Deembedding

Impedance deembedding is the process of extracting the sought impedance from a measurement by mathematically compensating for known parasitic impedances. This can be considered a form of instrument calibration for the specific measurement setup.

The unwanted impedances are commonly parasitic impedances such as series resistance and inductance stemming from cable length, or parallel capacitance stemming from conductor proximity. If there are other intentional elements in the measurement circuits such as connectors, diodes and fuses, the impedances they impose on the measurement circuit should also be "deembedded" from the measurement results.

Impedance measurement instruments include some type of setup compensation depending on the measurement method in use. For most measurements open-short-load calibration is preferred as it enables measurement of the full S-parameter matrix (see (2.15)).

In the case of the shunt-thru and series-thru methods (see 3.3.1 and 3.3.2 respectively), only the transmission gain ($\bar{S}_{21}$, see 2.1.7) is required [6]. Because the parasitic impedances are in series with the DUT, they can be measured and compensated for simply by shorting the two DUT connectors, simplifying the calibration procedure.

The best approach is to design the physical measurement circuit so as to need as little deembedding as possible. This results in the highest contrast between the sought impedance and any parasitic impedances. A common example of this is 4-wire measurements, that are used when the DUT resistance is on the same order of magnitude as the resistance of the test leads, i.e. very small. 4-wire measurements circumvent this problem by having separate leads for the test current and the voltage measurement.

2.1.7 Scattering Parameters

Scattering parameters is a term used mostly in the context of Radio-Frequency (RF) engineering and other electrical engineering domains at high frequencies.

S-parameters present a way to abstract a complex electrical system into a "black box" with a set number of electrical ports. When an AC signal is transmitted from a port i to a port j (may be the same in the case of "reflection"), the resulting gain and phase shift of the signal is expressed in the complex parameter $\bar{S}_{ij}$. I.e. $\bar{S}_{ij}$ is the specific transfer function for the transmission of any signal from port i to port j.

$$\bar{b}_i = \bar{S}_{ij}\bar{a}_j \tag{2.14}$$

Where $\bar{a}_j$ is the input signal and $\bar{b}_i$ is the output signal.

S-parameters for a multi-port system are represented in an $n \times n$ where n denotes the number of input ports. The S-matrix for a two-port network (e.g. a battery with a negative and positive pole) is written as

$$\begin{bmatrix} \bar{b}_1 \\ \bar{b}_2 \end{bmatrix} = \begin{bmatrix} \bar{S}_{11} & \bar{S}_{12} \\ \bar{S}_{21} & \bar{S}_{22} \end{bmatrix} \begin{bmatrix} \bar{a}_1 \\ \bar{a}_2 \end{bmatrix} \tag{2.15}$$

where

- $\bar{S}_{11}$ is the input port reflection coefficient.
- $\bar{S}_{22}$ is the output port reflection coefficient.
- $\bar{S}_{12}$ is the input port transmission coefficient (or "reverse voltage gain")
- $\bar{S}_{21}$ is the transmission coefficient (or "forward voltage gain")

Here, diagonal parameters are "reflection coefficients" as the signal enters and exits the two-port system at the same port (i.e. $\bar{a}_1$ to $\bar{b}_1$ and $\bar{a}_2$ to $\bar{b}_2$). Off-diagonal parameters are "transmission coefficients" as the signal is "transmitted" from one port to another (i.e. $\bar{a}_1$ to $\bar{b}_2$ and $\bar{a}_2$ to $\bar{b}_1$)[7].

3
Method evaluation

There are a number of methods used for measuring impedance on DC-biased systems. Each method exhibits different pros and cons. In this chapter, the most promising methods are presented and conclusions are drawn on which methods to implement.

3.1 Voltage-current measurement with transformer probes

This method is presented in [8] and [3]. The measurement (Figure 3.1) is conducted with voltage and current probes connected to a VNA from which impedance is calculated using (2.1).

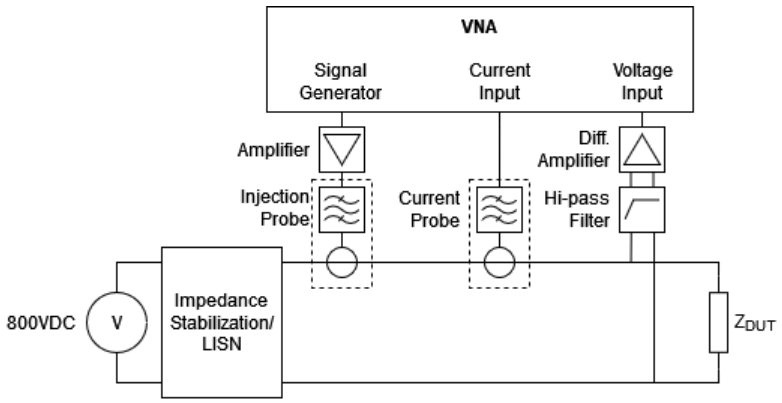

Figure 3.1: Diagram of the direct measurement method.

3.1.1 Voltage probe

Voltage is measured through a DC-blocking high-pass filter. This enables the measurement of the injected AC signal without the system's high voltage DC or low-frequency (LF) components damaging the amplifier or interfering with the signal. The fact that the signal is buffered by an external high impedance differential amplifier means the signal receiver affects the measurement minimally. The absence of a grounding connection common to the other injection and receiver ports means that ground loops are eliminated as well. These would otherwise affect low impedance measurements at low frequencies.

Note that for the voltage measurement, the high voltage DC-bias is blocked by the filter. This protects the amplifier's low attenuation, low-voltage input. If a high voltage differential amplifier with built-in all-band attenuation is used (such as the Tektronix THDP0200 with its input attenuation of 500x in its 1.5 kV mode[9]), the AC signal will be very small and difficult to measure accurately.

3.1.2 Current probe

The small signal current can be measured either with a current-sensing shunt resistor or a transformer-based measurement probe.

3.1.2.1 Resistance-based

For the shunt resistor case, a differential probe would measure the voltage across the resistor as in Figure 3.2. The value of the resistance will determine the signal strength ratio between the current measurement and the voltage measurement. A larger resistance leads to a larger current sensing signal amplitude, but also a smaller voltage sensing signal amplitude for the same injected power. This can be tuned for a given DUT impedance in order to obtain the best signal-to-noise ratio for each voltage or current receiver without overloading them.

The Bode 100 has settable input attenuation on each receiver to prevent receiver overloading at a given injected power. The downside to this is that the signal power is lost in the attenuator. By tuning the current shunt resistance, the signal strength of the current signal receiver can be transferred to the voltage signal receiver, and vice versa.

The Gamry Reference 3000 utilizes a current sense shunt resistor and is able to multiplex resistances in decades from 50 mΩ to 500 MΩ for the best measurement accuracy[10].

3.1.2.2 Inductance-based probes

An important consideration in the use of inductive coils is their susceptibility to external and common mode noise. The injected AC voltage can easily couple to the output of the current probe if the probe is placed on the positive pole. This effect is small but increases with frequency. It is recommended to conduct the measurement on the grounded negative pole of the DUT[11], however grounding the DUT would in this case mean an increased risk as a single isolation fault can cause a catastrophic failure.

Rogowski coils are a common inductive current measurement probe. The investigated coils were however not precise enough for the application. For example, the Teledyne LeCroy T3RC0120-UM has a noise floor of 70 mA and a limited bandwidth

of 34 Hz − 30 MHz.[12].

Reference [2] used a Pearson 2877 wideband current monitor for impedance measurements. Two similar current probes were evaluated and the results can be seen in Section 6.3.2.

3.1.3 Signal injection

The AC sweep signal is injected through a high-voltage interface, usually an injection transformer.

There are a number of injection transformers available on the market; however, none have been found that are suitable for 800 V systems. Most also lack satisfactory bandwidths. For the application, designing one or more custom transformers will be required. To measure the complete frequency range, multiple measurements with transformers optimized for different frequency ranges will be required. The designing of such transformers is outside the scope of this work.

Depending on the topology of the current probe, it may also be possible to utilize a second measurement probe ”in reverse” to induce the excitation current in the measurement circuit. This is however not investigated in this thesis.

It is possible to use a capacitor pair for signal injection, foregoing the injection transformer. This approach is discussed further in section 3.2.

3.2 Voltage-Current Measurement with DC Blocking Capacitors

In [2], Per Widek used a custom HV interface for high voltage battery measurements with a PSM3750 Frequency Response Analyzer (FRA). This method uses the same voltage and current measurement principle as discussed in section 3.1, only that it utilizes capacitive interfaces also for signal injection and current measurement. The voltage measurement is practically identical to the one in section 3.1.

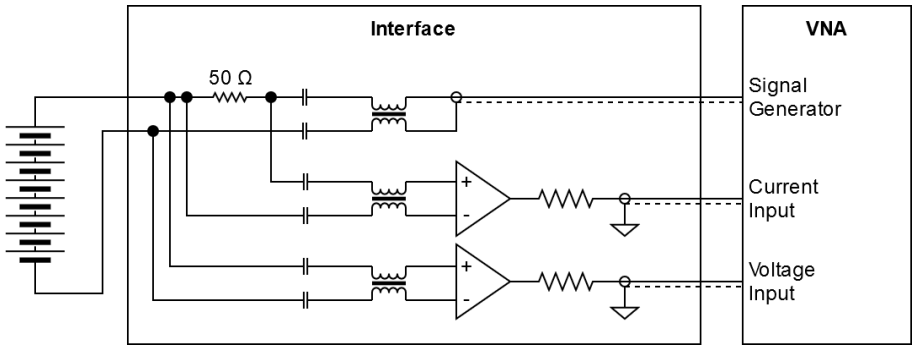

Figure 3.2: Diagram of Per Widek's differential capacitor interface [2].

In this method (see Figure 3.2), the signal generator of the FRA injects a swept-frequency signal across the DUT through a pair of DC blocking capacitors and a common mode choke (CMC). The current measurement is implemented independently and consists of a 50 Ω shunt resistance, the voltage over which is measured by a differential amplifier. The input of the amplifier is isolated by the use of capacitors and conditioned with a common mode choke. The DUT voltage measurement is conducted identically to the voltage measurement over the current shunt.

Although not specified by Widek, it is presumed that both amplifiers have a high input impedance and are mounted on the interface PCB as close to the agitation signal circuit as possible.

3.2.1 Limitations

The estimated bandwidth of the interface is approximately 600 Hz − 1 MHz. This bandwidth was determined by comparing impedance measurements of a capacitor with and without the interface [13]. Little information on the implementation of the method is available beyond the diagram in Figure 3.2. The interface's practicality and bandwidth-limiting factors are unknown without further investigation.

At low frequencies, Widek encountered changes in permittivity within the blocking capacitors leading to changes in their capacitance. This is acceptable as long as the per-frequency capacitance is unchanged from the time of calibration to the time of measurement.

If there are other changes in setup impedance in-between calibration and measurement (e.g. due to the blocking capacitors' applied DC bias or temperature) the impedance difference will be interpreted as part of the DUT impedance.

The lower impedance limit can possibly be reduced by increasing the DC block capacitance [13].

For high frequencies, the DC-blocking capacitors are expected to form resonant circuits with the parasitic inductances present in the setup. These resonances are not

the main issue, but rather a symptom of large parasitic impedances which will, by themselves, make accurate measurements difficult. In the case of capacitor size selection there commonly is a trade-off between high capacitance and low parasitic series inductance. The effects of the different types of parasitic impedances are discussed further in the thesis.

Another possible issue at high frequencies is signal reflection. Reflection can be especially prominent in the traces leading to the high impedance differential amplifiers due to the large impedance mismatch. Impedance mismatches will also be present in the rest of the circuit as well as in the leads [14]. Reference [14] mentions reflection as a major issue with measuring at high frequencies with conventional EIS methods.

3.2.2 Safety Aspects

As the capacitors are to be biased with a high DC voltage, their charge and discharge needs to be controlled. When connected to the HV system, the current through them needs to be limited in order to ensure high inrush currents do not damage components in the circuit. Attention needs to be paid where the current is restricted so that low voltage circuits are not subjected to high voltage transients on connection. In addition to this, the capacitors need to be discharged when the DUT is disconnected in order to prevent potential electric shock due to residual energy stored in the capacitors.

3.2.3 Transformer Coupling

Transformers are a common way to achieve DC isolation in HV EV systems. For the current injection and current measurement ports respectively, a transformer would be able to replace the DC blocks, current shunt and CMCs, leading to a solution resembling Figure 3.1. Voltage measurement is less trivial as it would require a transformer winding (in series with a DC-blocking capacitor) to shunt the DUT with its low HF impedance. This would divert a portion of the injected current and lead to a design where either the current or voltage measurement is affected by impedances inherent in the other.

An important aspect to consider for a transformer solution is that the core permeability is affected by the injected power (through flux density) and its frequency. This change in permeability affects the transformer's inductance[15]. Saturating the core material leads to non-linear transformer behaviour and will negatively impact the measurement.

Communication isolation transformers such as the Pulse Electronics HM2113ZNL or Coilcraft ZA975X can be used for the application. These transformers are designed for low power signals and frequencies between the 100s of kHz to tens of MHz. Lower and higher frequency transformers will be required for measurements in other

frequency ranges. Due to availability, only the HM2113ZNL is investigated further in Section 5.2.1 and Section 6.2.1.

3.2.4 Conclusion

Compared to the one- and two-port methods (see 3.3), where one or both signal receivers are connected internally inside the measurement instrument itself, the voltage-current method is the most flexible. It is in theory adaptable to all types of measurements. Amplifiers and filters can be changed depending on requirements, the signal generator can be disconnected and voltage-current measurements can be carried out on source-load systems as well.

There are examples of successful battery impedance measurements using capacitive interfaces. A benefit is their simple design and behaviour. However, they require additional safety circuits to safely charge and discharge the interface capacitors.

3.3 One- and two-port methods

The simplest methods of measuring impedance is by using the signal generators and signal receivers built-in to the measurement instrument with a minimal amount of peripheral equipment.

These measurements are made by inferring impedance from $\bar{S}_{11}$ (reflection) or $\bar{S}_{21}$ (gain-phase) measurements (see 2.1.7). The benefit is that the methods only use one and two ports respectively without requiring any equipment other than a fixture.

3.3.1 Shunt-through method (two-port)

The 2-port shunt-through method is recommended for impedance ranges of $1\,\mathrm{m\Omega} - 100\,\Omega$[16][6][17], but can be used for up to $1\,\mathrm{k\Omega}$ using the Bode 100[18]. This impedance range is the best match with the expected full battery impedance range of $20\,\mathrm{m\Omega} - 1\,\mathrm{k\Omega}$. The upper limit relates to the noise-level and dynamic range of the Bode 100 measurement instrument[18]. The range can be modified and increased further by the use of series resistors and port extension as presented in [18]. Landinger et al. [14] utilize the 2-port shunt-through method to measure the impedance of a 18650 li-ion cell in a frequency range of $1\,\mathrm{kHz} - 300\,\mathrm{MHz}$.

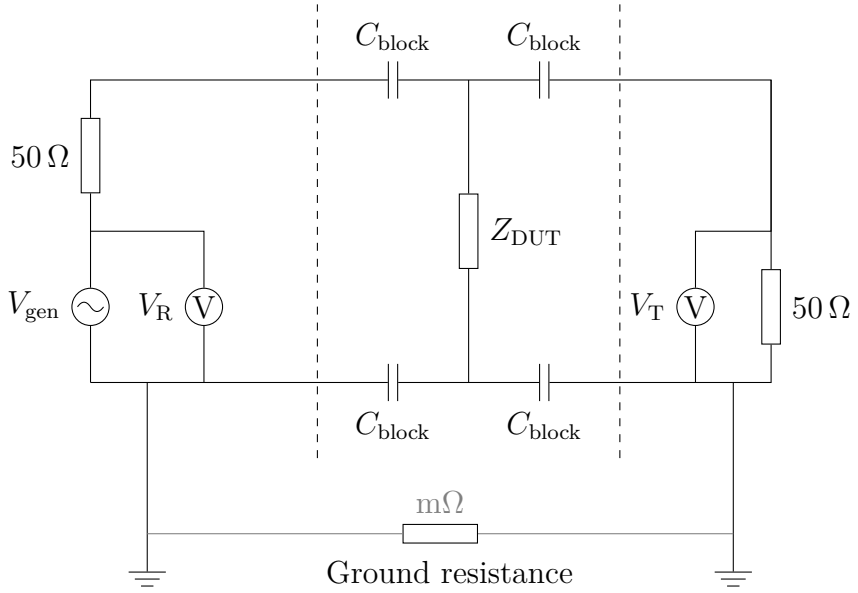

Figure 3.3: Diagram of the 2-port shunt-through method using the capacitor interface. The internal grounding connection in the Bode 100 is also visualized.

In the Bode 100 the measurement is conducted on a voltage-current basis, where V_{T} measures the voltage across the DUT, and

$$I = 50(V_{\text{R}} - V_{\text{T}}) \tag{3.1}$$

is the current through the DUT.

In 3.3, V_{T} denotes the receiver of the *transmitted* signal, while V_{R} denotes the receiver of the *reflected* signal. This nomenclature carries little importance as there is no true signal directionality involved. The circuit function can be easily understood without accounting for signal scattering (see 2.1.7). VNAs measuring at higher frequencies usually use a directional coupler to separate the reference signal, reflected signal and transmitted signal before measurement.

A simpler alternative to the shunt-thru method is the 1-port "reflection" method. This method is discussed further in Section 3.3.3.

To provide full battery isolation and measurement accuracy in the full battery application, the implementation by Landinger et al. needs to be modified (Figure 3.3). An additional DC-blocking capacitor should be placed in between the DUT ground and both ports to ensure safety in case one isolation barrier breaks and the measurement has to be aborted.

A ground loop is formed by the connection of the two port grounds as they are already connected internally in the instrument (see Figure 3.3). When measuring very small impedances at low frequencies, the impedance in the ground connection may be comparable to the DUT. With a low frequency signal this may result in a

potential difference between the two port grounds, leading to measurement distortion.

According to [3] and [6], ground loops should be suppressed by the use of a common mode choke or a differential amplifier on port 2. This will suppress the common mode current passing through the parasitic ground-ground impedance. If this is not done, [17] claims significant measurement errors can be present for low impedance measurements at frequencies up to 100 kHz. For DUTs of higher impedance, the differential-mode voltage exceeds the common-mode voltage inflicted by the ground loop

3.3.2 Series-through method (two-port)

Omicron Lab recommends the series-through method for DUT impedances of 1 kΩ to > 1 MΩ. Due to this it is likely the preferred method for common-mode impedance measurements.

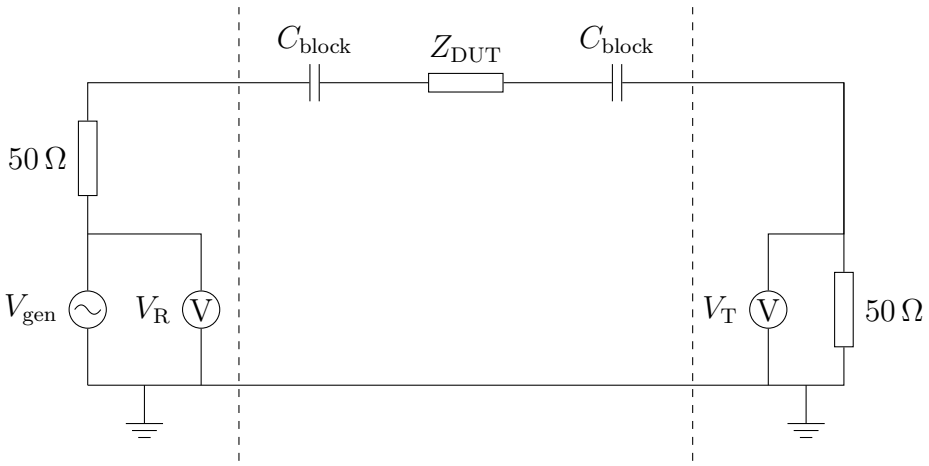

Figure 3.4: Diagram of the 2-port series-through method.

As seen in figure 3.4, the ground connection between the two ports cannot pass through the DUT. The complex geometries of cell, module or battery DUTs can create large conductor loop areas with parasitic inductance or capacitance that are likely to deteriorate the measurement.

3.3.3 Reflection method (one-port)

When using the Bode 100, the one-port reflection method (Figure 3.5) is similar to the two-port shunt-thru method. Here the signal transceivers (V_{R}, V_{T} in Figure 3.3; V_1, V_2 in Figure 3.5) are connected internally and only a single port conects to the interface or DUT.

As the injected current is conducted through the same path and series parasitic impedances as the voltage measurement, it will distort the voltage measurement.

Thus, Omicron Lab's recommended impedance range for the one-port method is 500 mΩ to 10 kΩ, i.e. higher than that of the shunt-thru method.

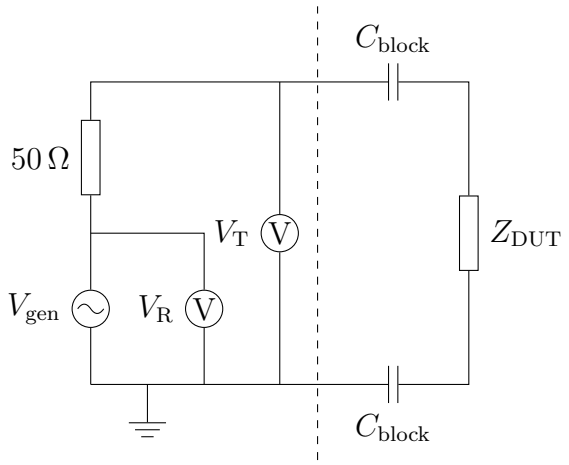

Figure 3.5: Diagram of the 1-port reflection method with Bode 100 internal connections.

In Figure 3.5 the receivers are again denoted V_{R} and V_{T}. This is purely to keep consistency with figures 3.4 and 3.3.

3.3.4 Conclusion

The two two-port methods are the simplest to implement as they do not require any active components in the measurement. With a thought-through design, the series-through and shunt-through interfaces can be combined, enabling the evaluation of the different methods on the same hardware.

3.4 Transformer Interface

Mazzola et al. [19][20] present an approach of measuring impedance directly with an impedance analyzer through an isolating transformer (Figure 3.6). Some type of DC blocking device is required so as not to short-circuit the high voltage system with the secondary winding of the transformer. In this case a blocking capacitor is used.

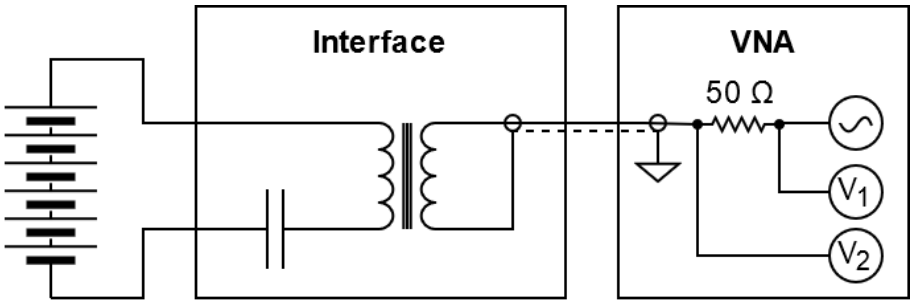

Figure 3.6: Diagram of the transformer-based method proposed by Mazzola[19][20].

The upper impedance limit of this method is determined by the open-circuit impedance of the transformer and the accuracy of the impedance measuring instrument. Should the impedance of the DUT be much greater than the open circuit impedance, there may not be enough precision in the instrument to determine the DUT impedance. As the open circuit impedance decreases with increasing frequency due to conductor-conductor or transformer distributed capacitance[15], the range of measurable impedance is reduced as well.[20]

The lower impedance limit is determined by the short-circuit impedance of the transformer and the accuracy of the impedance measuring instrument. Should the impedance of the DUT be much lower than the short-circuit impedance, there may not be enough precision in the impedance measurement to determine the DUT impedance. As the short circuit impedance increases with increasing frequency due to conductor and transformer leakage inductance, the range of measurable impedance is reduced as well. Open/short measurements can be conducted to determine these measurement limits[20].

3.4.1 Frequency

The frequency ranges of the evaluated methods are summarized Figure 3.7.

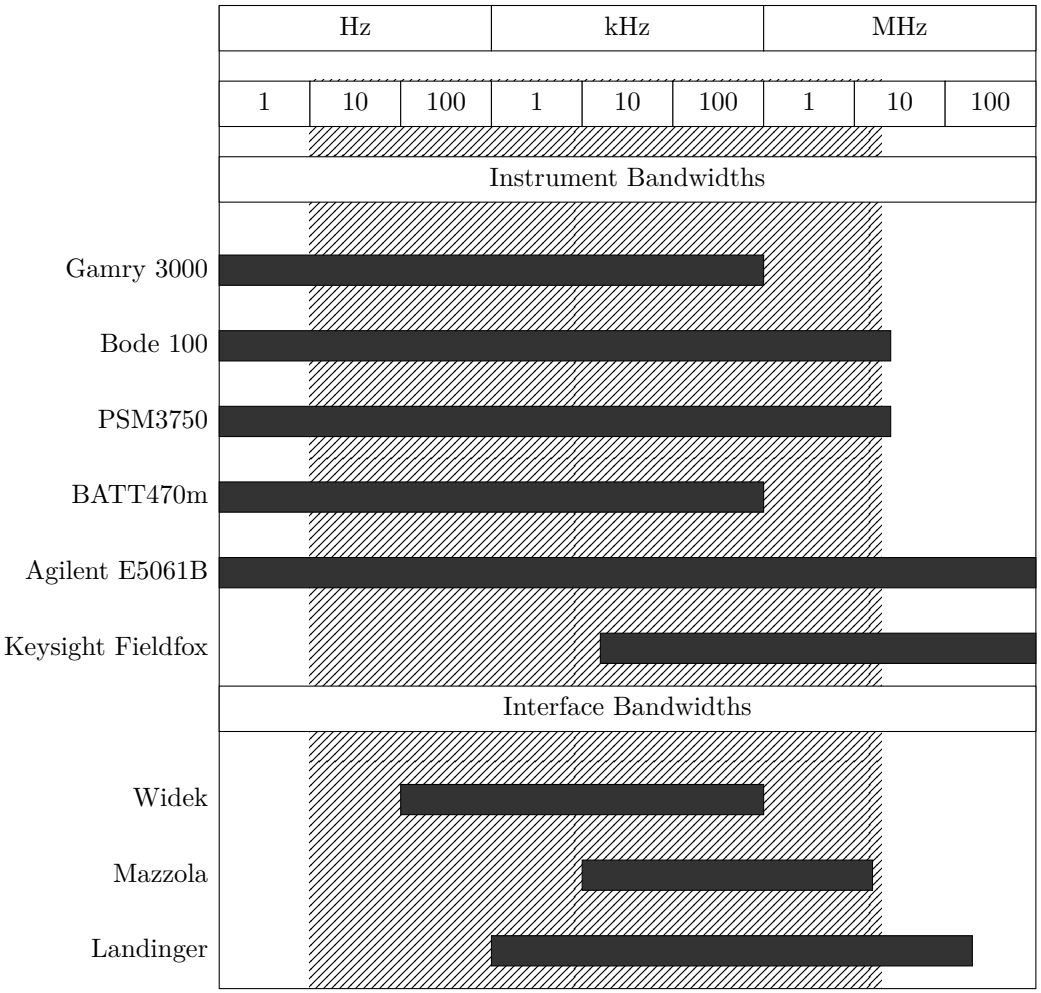

Figure 3.7: Usable frequency ranges of the investigated methods according to their respective sources.

4

Electrical Modelling

Electrical modelling was employed in order to gain a better understanding of the methods and to enable isolated investigation of different circuit behaviours.

4.1 Battery Model

In this section, a battery model is constructed for use within the 1 kHz – 100 MHz range. It is fitted to cell-level EIS data previously collected by VCC.

4.1.1 EIS Reference Data

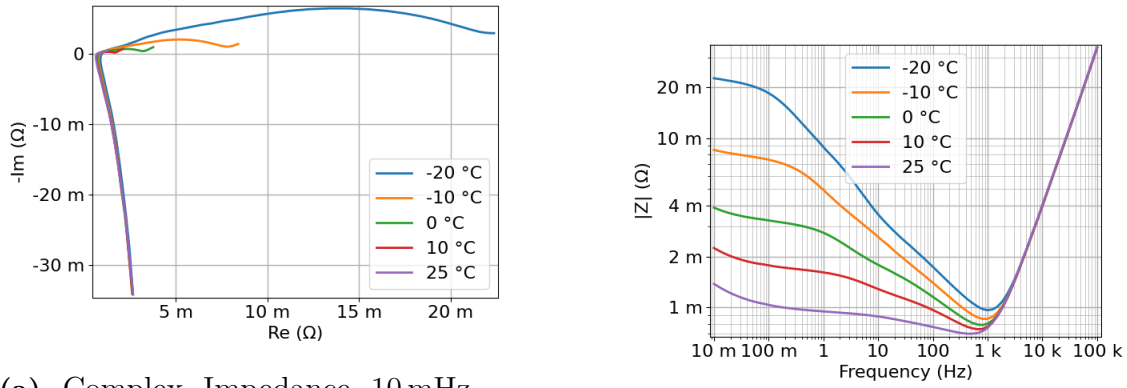

(a) Complex Impedance 10 mHz – 100 kHz.

(b) Impedance magnitude.

Figure 4.1: EIS Data extracted from a CMA cell at different temperatures.

Figure 4.1 shows the EIS data collected by VCC. The frequency ranges from 10 mHz to 100 kHz and thus fails to capture the resonant behaviour expected at higher frequencies. This means it is not useful for measurement verification above 100 kHz. A model based on the data was constructed regardless and used for interface design as there was no better impedance estimation available.

As can be seen in both the complex and amplitude figures in Figure 4.1, cell chemistry modelling starts becoming irrelevant above 1 kHz. This is due to the increasing dominance of the cell's inductance.

4.1.2 Single Cell Model Construction

In [14], where frequencies above 1 kHz are investigated, a very simple RL circuit (Figure 4.2) is used as a battery model. The model seen in Figure 4.2 contains element values fitted to the EIS data.

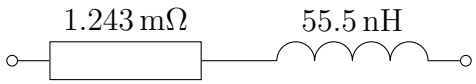

Figure 4.2: RL battery cell model.

Figure 4.3a compares the EIS data collected from the cell, with the values replicate by the circuit model after curve fitting. It is evident that this model contains too few elements for accurate modelling of the cell's complex impedance.

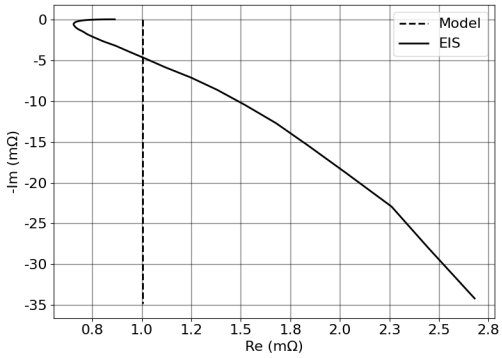

(a) Complex Impedance of simple cell model 10 mHz − 100 kHz.

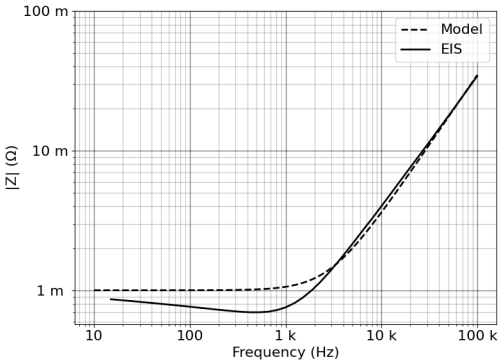

(b) Impedance magnitude of simple cell model.

Figure 4.3: Impedance results from RL battery cell model.

In order to improve low frequency accuracy, a series capacitance is added. To improve complex impedance accuracy at higher frequencies, an R ‖ L link was added. The parameters of the new model in Figure 4.4 were obtained by curve fitting to the EIS data. This was done in the Python programming language using the `scipy.optimize.curve_fit()` function.

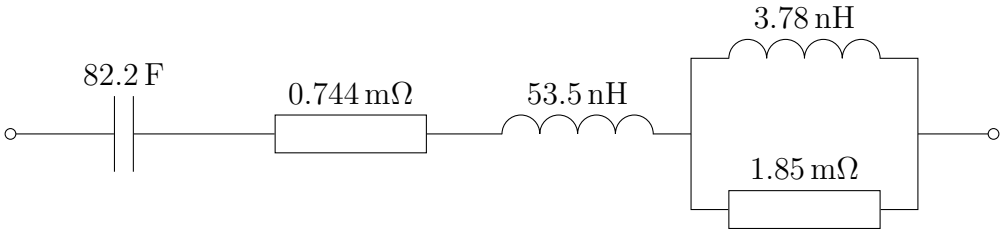

Figure 4.4: CRLRL Battery model with curve-fitted parameters.

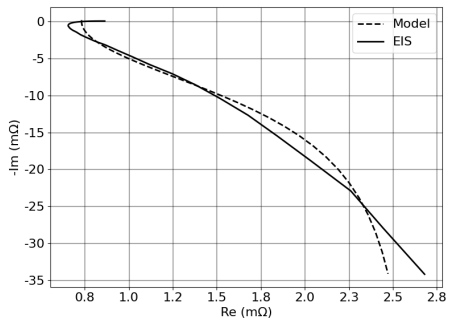

(a) Complex Impedance of CRLRL model 10 mHz − 100 kHz.

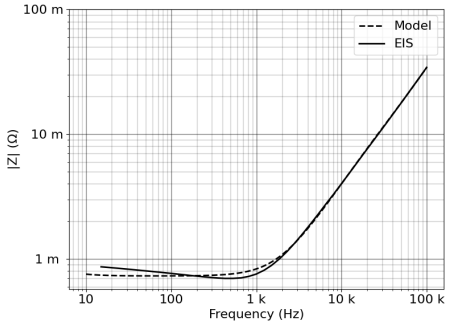

(b) Impedance magnitude of CRLRL model.

Figure 4.5: Impedance results from CRLRL battery model.

The result in Figure 4.5 is a better fitting model; however, the complex impedance accuracy can be improved further by the use of an additional R ∥ L link. The result is the model seen in Figure 4.6. Again, the element parameters were obtained by curve fitting to the EIS data.

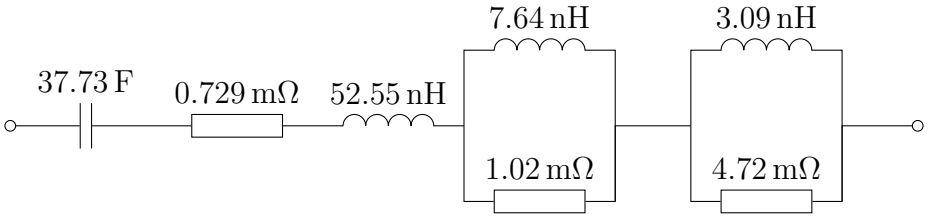

Figure 4.6: CRLRLRL Battery model with curve-fitted parameters.

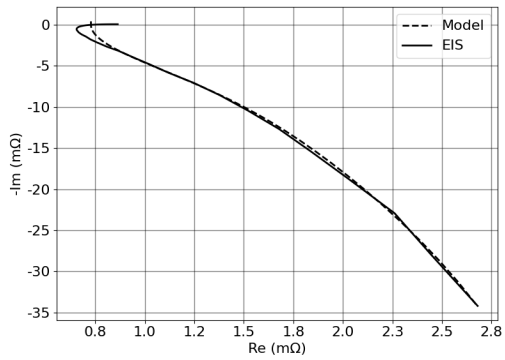

(a) Complex Impedance of CRLRLRL model 10 mHz − 100 kHz.

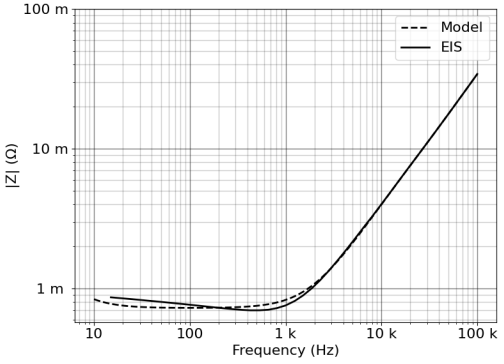

(b) Impedance magnitude of CRLRLRL model.

Figure 4.7: Impedance results from the CRLRLRL battery model.

Again, for frequencies higher than 100 kHz where reference data on the cells to be investigated is missing, the DUT behaviour will no longer conform to these models and additional elements may need to be considered.

Frequencies down to 10 Hz are also of interest. These can be represented with more conventional battery model elements. As the bandwidth of the interface to be implemented was not expected to reach below 1 kHz, this frequency range is left for future work.

4.2 Two-port Shunt-through Model

The two-port shunt-through method was modelled in LTSpice.

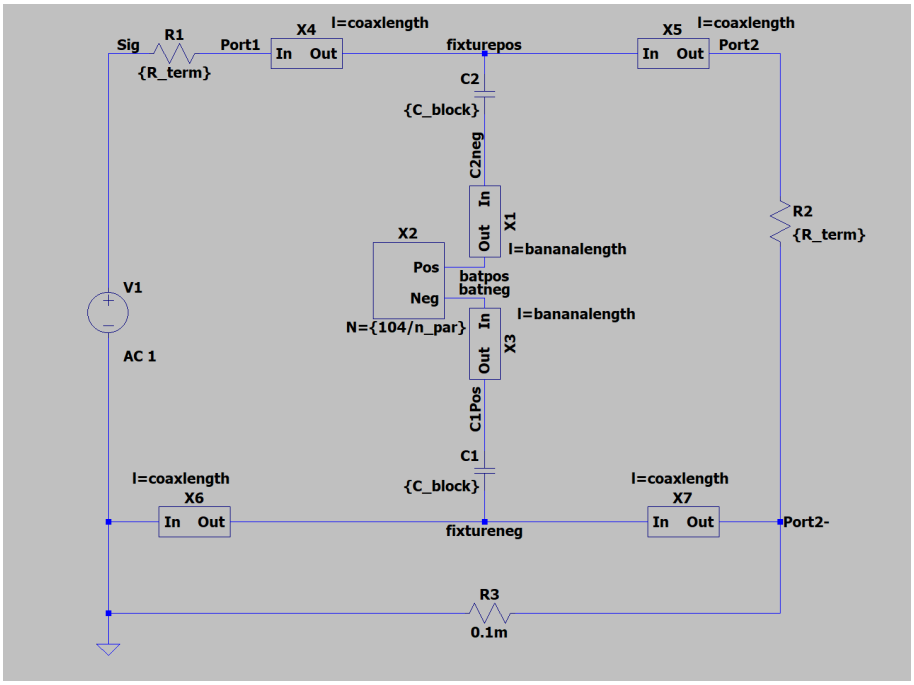

Figure 4.8: LTSpice model of the shunt-through method.

The model in Figure 4.8 contains the signal generator and measurement circuits of the Bode 100 VNA. The Bode 100 contains one signal generator and two signal receivers which measure AC voltage magnitude and phase. Signal receiver 1 measures the voltage over V1, i.e. the signal generator. Signal receiver 2 measures the voltage across the terminating resistor R2. Coaxial and banana plug cables are modelled as simple RL loads.

The capacitance between positive and negative conductors is omitted as it is not critical for the current purpose of demonstrating other aspects of the measurement. This capacitance is an important limiter of the frequency range which can be measured, and should be included in future models.

For the circuit in Figure 4.8, the DUT impedance $\bar{Z}_{\mathrm{DUT}}$ is expressed as;

$$\bar{Z}_{\mathrm{DUT}} + 2\bar{Z}_{\mathrm{block}} = \frac{\bar{Z}_0}{2}\frac{\bar{S}_{21}}{1-\bar{S}_{21}} \tag{4.1}$$

according to [17]. $\bar{Z}_0$ is the characteristic impedance of the test setup. When using the built-in termination resistors of the Bode 100, $\bar{Z}_0 = R_{\text{termination}} = 50\,\Omega$.

Furthermore, according to [21], the forward gain $\bar{S}_{21}$ can be expressed as

$$\frac{\bar{V}_{\text{out}}}{\bar{V}_{\text{gen}}} = \frac{\bar{S}_{21}}{2} \tag{4.2}$$

Using (4.1) and (4.2), $\bar{Z}_{\text{DUT}}$ can be expressed as

$$\bar{Z}_{\text{DUT}} = \bar{Z}_0 \frac{\bar{V}_{\text{out}}}{\bar{V}_{\text{gen}} - 2\bar{V}_{\text{out}}} - 2\bar{Z}_{\text{block}} \tag{4.3}$$

where $\bar{V}_{\text{gen}}$ is the voltage across the voltage source, before the $50\,\Omega$ input resistor[8].

Note that in (4.3), $\bar{Z}_{\text{block}}$ is deembedded from the measurement to extract $\bar{Z}_{\text{DUT}}$. For more on deembedding, see section 2.1.6.

5
Method

This section first presents what instruments were used to measure and collect impedance data (Section 5.1). Secondly, it presents the two prototype interfaces that were used to verify the methods using passive components (Section 5.2). Lastly, it presents the interface and methods used to conduct measurements on energized cells (Section 5.3).

5.1 Impedance Measurement Instruments

Two impedance measurement instruments were used in this thesis; A Bode 100 VNA manufactured by Omicron Lab, and a FieldFox handheld RF analyzer manufactured by Keysight.

The Bode 100 is the more economical alternative and is designed for impedance measurement in a frequency range of 1 Hz to 50 MHz. Common use-cases are resonance and impedance analysis of passive elements (e.g. capacitors, inductors and crystals) and stability analysis of active circuits (e.g. power converters).

The Keysight FieldFox is a handheld RF analyser and operates in a frequency range of 30 MHz to 6.5 GHz. Common use-cases are antenna and cable analysis, Spectrum analysis and 5G/LTE testing. The FieldFox is used to enable impedance measurements beyond the 50 MHz limit of the Bode 100.

5.2 Passive DUT Measurements

In this section, the measurement setups used during measurements on passive components are presented.

5.2.1 Prototype Transformer Interface Setup

Two simple transformer interfaces were tested. The first is the Bode 100 "Wideband Injection Transformer" (B-WIT) and can be seen in Figure 5.1a. The second consists of an HM2113ZNL signal transformer soldered onto a breadboard and can be seen in Figure 5.1b.

The open-circuit and short-circuit impedances of the interfaces were measured in order to evaluate their viability for use in the transformer-based interface presented

in Section 3.4.

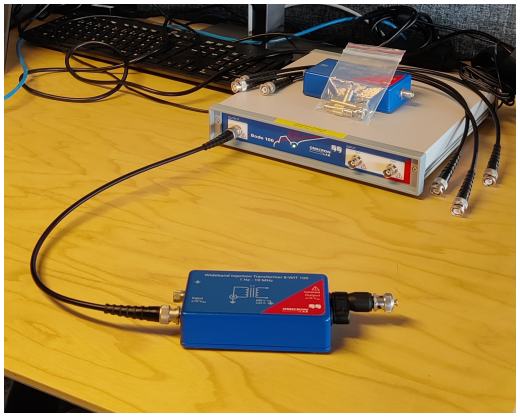

(a) B-WIT setup

(b) HM2117ZNL setup

Figure 5.1: Interface transformer impedance measurement setups.

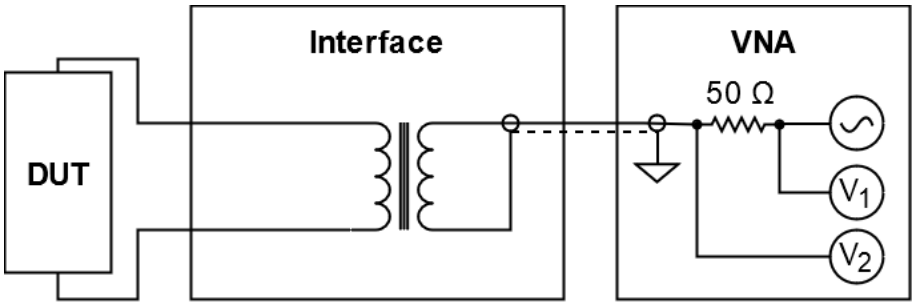

Figure 5.2: Diagram for the transformer prototypes without DC-blocking components.

The schematic diagram of the two transformer prototypes can be seen in Figure 5.2

5.2.2 Prototype Capacitive Interface Setup

A crude prototype capacitive interface (see Figure 5.3) was tested on passive DUTs without DC bias. This prototype consisted of two 2.2 mF axial electrolytic capacitors connected to the measurement instrument and the DUT using screw terminals and a breadboard.

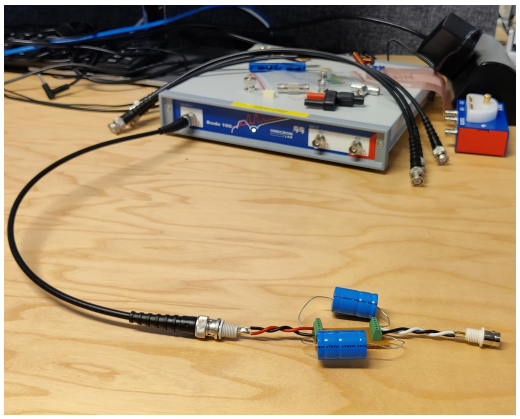

(a) Coaxial setup.

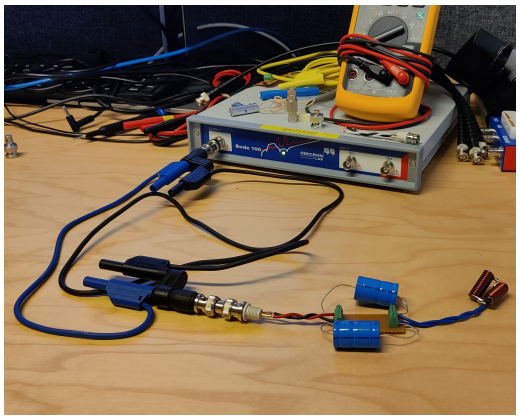

(b) Banana lead setup.

Figure 5.3: Capacitive prototype interface setups.

5.2.3 Reference DUTs

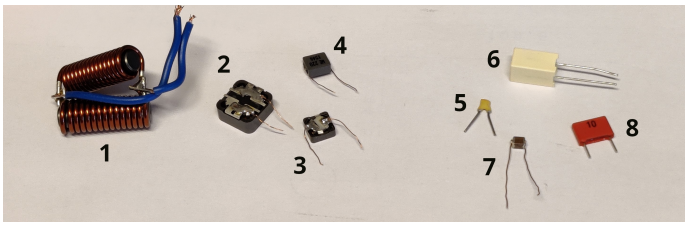

Figure 5.4: Passive components used for interface verification.

A varied set of inductors and capacitors were used in order to evaluate the usability of the interface prototypes. These can be seen in Figure 5.4. DUT number 1 is the inductor designed to mimic the inductance of the full battery.

Table 5.1: Example DUTs and their parameters.

# in Figure 5.4[3]	L (μH)	C (μF)	Type
1	1.65	-	2p[1] Cylindrical Inductor
-	1.8	-	SMT[2] Inductor
4	18	-	SMT[2] Inductor
3	22	-	SMT[2] Inductor
2	100	-	SMT[2] Inductor
-	-	0.0001	Ceramic Capacitor
5	-	0.001	Ceramic Capacitor
-	-	0.01	Polyester Capacitor
8	-	0.1	Polyester Capacitor
6	-	4.7	Polyester Capacitor
7	-	4.7	ML[4] Ceramic Capacitor
-	-	2200	Electrolytic Capacitor

[1] Two parallelly soldered inductors.
[2] Surface Mount Techology.
[3] '-' entries are not present in Figure 5.4.
[4] Multi-Layered.

Note in table 5.1 that all inductors exhibit some capacitance, and all capacitors exhibit some inductance. These parasitics were not quantified here, but are hugely important for impedance measurement. This is especially true for the capacitors that exhibit considerable ESL and become inductive at relatively low frequencies (usually below 1 MHz).

5.3 Cell Level Testing

Cell level testing was conducted on lithium-ion pouch cells using a custom capacitive DC-blocking interface. The tests were conducted with the same pouch cells of the VCC CMA platform for which the EIS data was presented in Figure 4.1.

5.3.1 Cell Testing Interface Design

The cell testing interface was designed for measurements on single or multiple cells up to 40 V.

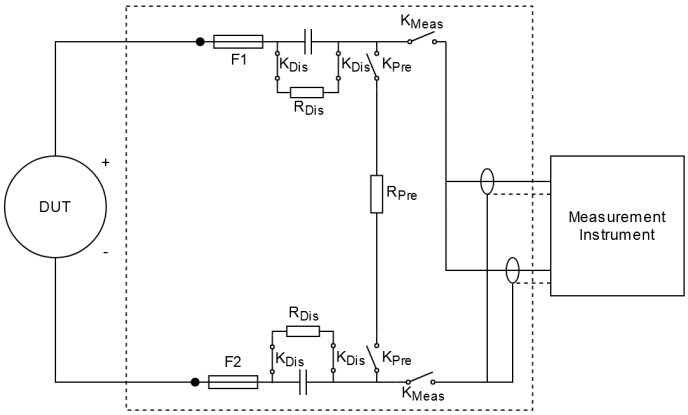

Figure 5.5: General overview of the interface design, where K: Relay, F: Fuse, R: Resistor.

The interface, see Figure 5.5, consists of two DC blocking capacitors with connectors to which the measurement instrument and the DUT can connect. Additional safety features are implemented:

- DUT connector fusing (F1, F2)
  - To prevent capacitor inrush current or short circuit currents from damaging the interface.
- Precharge circuit (K_{Pre}, R_{Pre})

  - To safely precharge the DC blocking capacitors before connecting the measurement ports. Inrush current would otherwise damage the 50 Ω port termination resistors inside the instrument.
- Discharge circuit (K_{Dis}, R_{Dis})
  - To safely discharge the energy stored in the capacitors when measurement is complete. Otherwise there is a risk of rapidly discharging the energy into sensitive equipment or to discharge it fast enough to damage the interface itself.
- Instrument Disconnection Circuit (K_{Meas})
  - To disconnect the measurement instrument from voltages that may damage it.
- Automatic precharge/measurement control circuit.
  - Designed to automatically control the precharge and measurement relays depending on the capacitor voltage.
  - This was not utilized in tests as manual control is faster to implement and unlikely to fail.
- Status, precharge and discharge indication LEDs
  - To ease troubleshooting and increase the detection rate of faults that may damage the equipment or persons.

Note that two types of relays are used in the circuit (Figure 5.5); normally open (NO) and normally closed (NC). When designing for high-voltage safety, it is important to consider when and where high voltage can be allowed. Selecting the correct relay types allow safety features like interface de-energization in case of power loss. More details on the interface operation sequence are presented in Sections 5.3.1.1, 5.3.1.2 and 5.3.1.3.

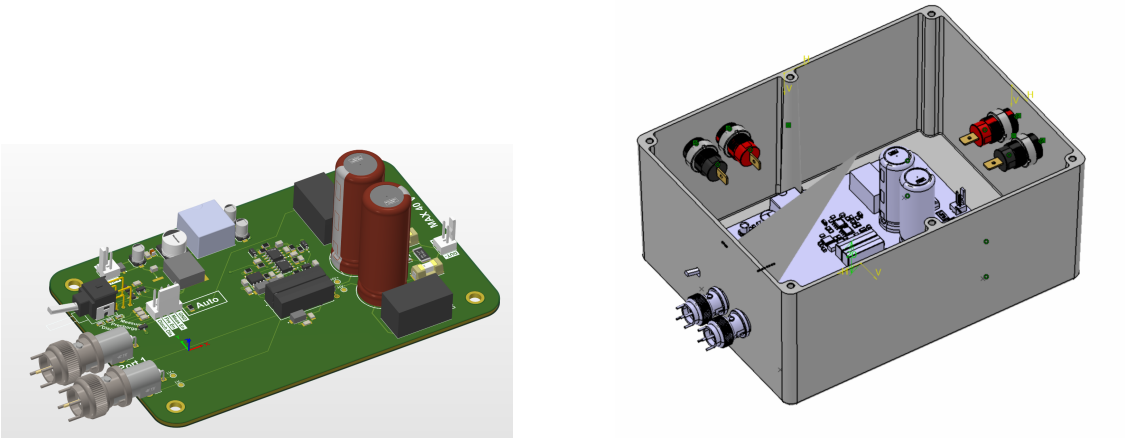

(a) LV capacitor interface circuit board.

(b) LV capacitor interface inside its aluminum enclosure.

Figure 5.6: LV Capacitor interface.

The board was designed for 2 mF 50 V capacitors to enable as low frequency measurements as practical. Doersam et al. used 200 μF and measured down to $\approx 1.7\,\Omega$ at 1 kHz[3]. As the cells and battery packs are expected to have a much lower

impedance at much lower frequencies; the larger capacitance is needed.

The circuit board is placed inside an aluminum enclosure with minimal openings to ensure best immunity to external noise. Attention was paid to not ground the BNC connectors by contact to the enclosure. This would, according to Doersam et al.[3], open up for measurement distortion by ground loops. As seen in section 6.3.1.1, this isolation seemed to have little significance.

The interface uses three modes, selectable with a three-position switch, to ensure safe operation:

- The discharge mode, where the interface capacitor charge is constantly depleted.
- The pre-charge mode, where the capacitors are safely charged to the DUT voltage.
- The measurement mode, where interface parasitic impedances are minimized to obtain best measurement accuracy.

5.3.1.1 Discharge Mode

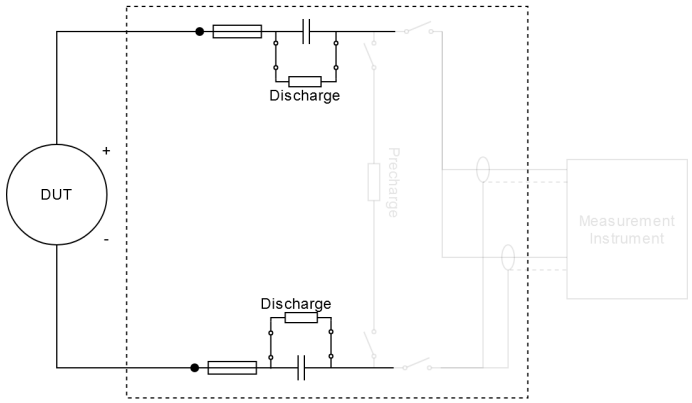

Figure 5.7: Discharge Mode.

The interface is in the discharge mode (Figure 5.7) whenever the power to the interface is turned off, or when the three-way switch is in the downwards ("discharge") position. This is the safe mode of the interface where capacitors are discharged and protected from short-circuits. The DUT and instrument sides are isolated in this mode.

In this mode, none of the relays are energized; their connection depends on if they are of ”normally open” (NO) type or ”normally closed” (NC) type.

The precharge relay and measurement relays are of NO-type. This means the precharge resistance and measurement instrument are disconnected from the ca-

pacitors in the discharge mode, and when the interface is unpowered.

The discharge relays on the other hand are of NC-type, meaning that they connect the discharge resistors to the capacitors whenever the interface is in discharge mode, or no power supply is connected.

5.3.1.2 Pre-charge Mode

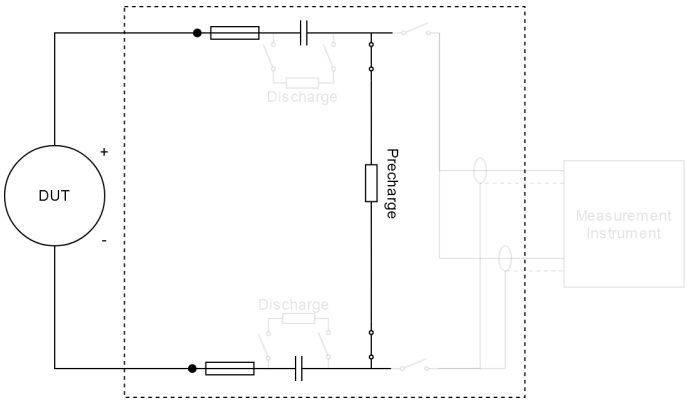

Figure 5.8: Pre-charge Mode.

The interface is in the pre-charge mode (Figure 5.9) whenever the interface is powered and the three-way switch is in the middle ("pre-charge") position.

During pre-charge, the discharge relays are energized, meaning the discharge resistors are disconnected. The measurement relays are still not energized to protect the instrument.

5.3.1.3 Measurement Mode

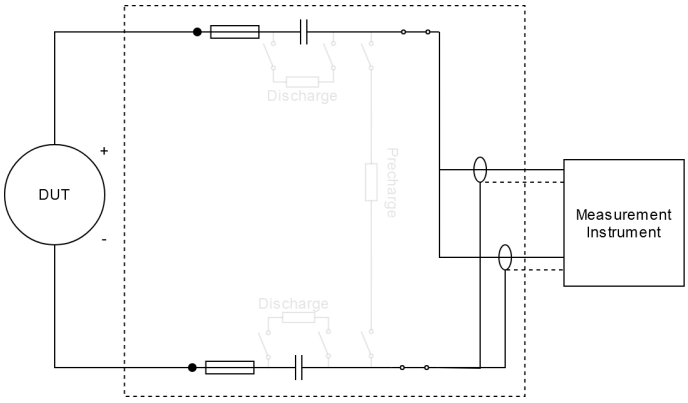

Figure 5.9: Measurement Mode.

The interface is in the measurement mode (Figure 5.9) when the interface is powered, and the three-way switch is in the upwards ("measurement") position.

In this mode, the discharge resistors are kept disconnected by the discharge relays. The pre-charge resistor is also disconnected by the pre-charge relay to not affect the measurements. Lastly, the measurement relays connect the measurement instrument to the measurement path.

5.3.1.4 Interface Versatility

A benefit of the interface design is that it is general enough to be used for all of the presented capacitive measurement methods with no modifications post manufacture.

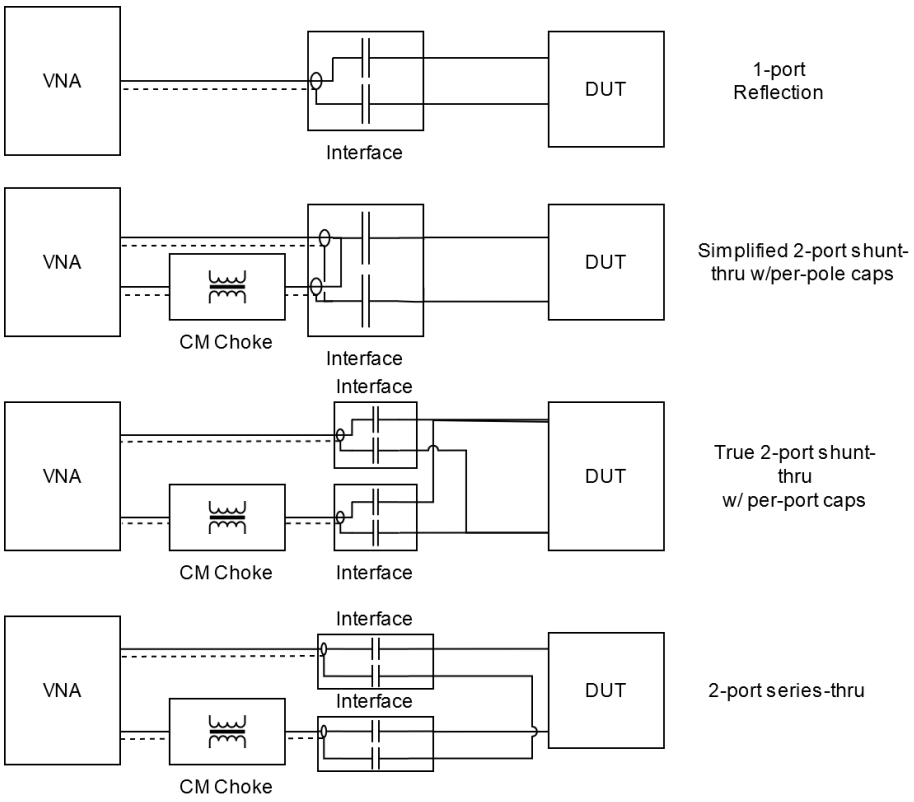

Figure 5.10: Setups for different measurement methods.

As seen in Figure 5.10, a single interface can be used to conduct 1-port and 2-port shunt-through measurements. Two additional solutions, which use two interfaces, are also shown. One is an alternative version of the shunt-through method; the other is a series-through method.

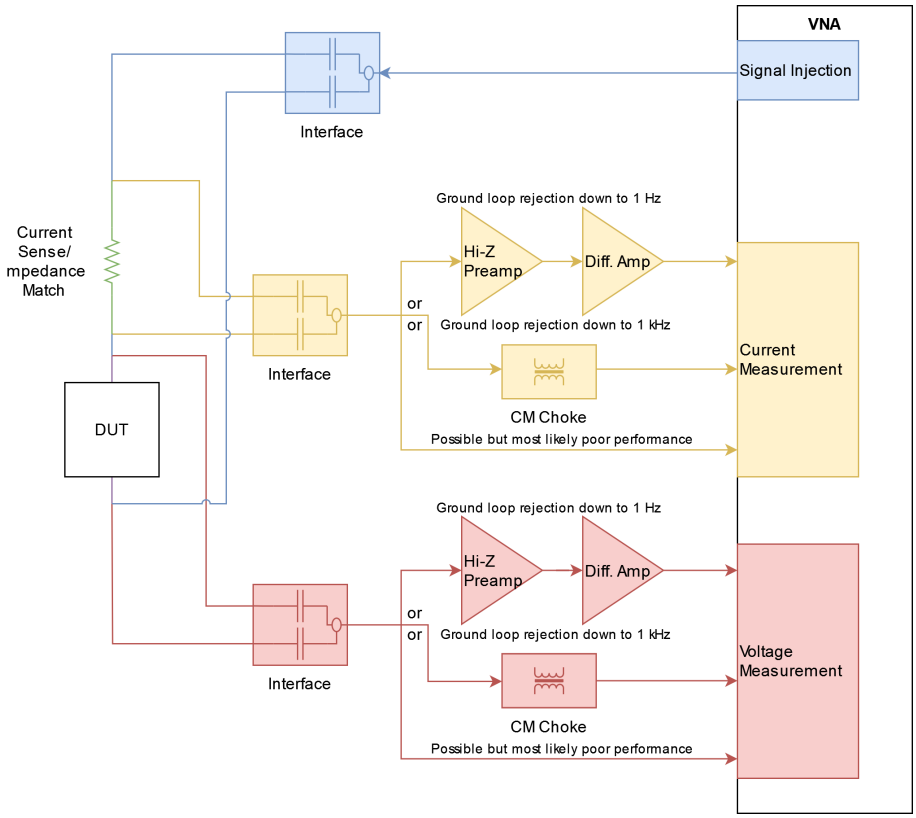

Figure 5.11: Proposed setup for Widek's method.

In Figure 5.11, an additional solution is shown where three interfaces are used. This resembles the interface used by Widek [2]. Different peripheral equipment such as amplifiers and filters can in this case be connected between the interface and the instrument.

Any amplifiers or filters need to be chosen properly if they are not to limit the bandwidth of the measurement. Common-mode and power supply noise entering an amplifier will be transmitted into the instrument receiver input. The noise sensitivity depends on the amplifier's Common-Mode Rejection Ratio (CMRR) and Power Supply Rejection Ratio (PSRR), respectively.

Note that the benefits of the Widek interface, such as minimal conductor length between DC-blocking capacitors and amplifier, are not retained with the presented interface. Additional safety aspects may also need to be taken into account, such as the equalization of potential between the measurement ports.

5.3.2 Testing Chamber and Jig

Figure 5.12: Single cell test setup.

The single cell tests were conducted in a temperature controlled chamber, see Figure 5.12, with a fully metallic enclosure. All non-metallic openings were covered, either with aluminum foil or aluminum mesh, for the purpose of blocking external EMI from entering the chamber. The cell was placed on an acrylic plate suspended $\approx 10\,\text{cm}$ above the metallic shelf of the test chamber in order to reduce the parasitic capacitance between the setup and the chamber. Movable cables and components were secured and positions were marked so as to minimize any changes to the setup inductance or capacitance in between calibration and measurement.

5.3.3 Test-specific Measurement Setups

Tests were conducted with different methods, equipment and temperatures for comparison.

5.3.3.1 Coaxial Length Comparison

At first the Bode 100 and FieldFox (presented in Section 5.1) were placed outside the chamber and were connected to the interface with 2 m BNC cables as seen in Figure 5.12. Later, in an attempt to reduce the setup series inductance and parallel capacitance, the Bode 100 was placed inside the chamber and connected to the interface with 0.5 m BNC cables.

5.3.3.2 One- and Two-port Method Comparison

The one- and two-port measurements were conducted by connecting one and both ports of the same interface respectively; as shown in Figure 5.10.

5.3.3.3 Voltage-current Measurement With Current Clamp

The same LV interface as before was used for current injection and voltage measurement through each BNC connection. The DUT current itself was measured with a current clamp on the negative DUT pole. The intention of the measurement was that it would reduce the measurement distortion incurred by parallel capacitance. The capacitance would otherwise divert some injected current past the DUT after it has been measured at the injection point.

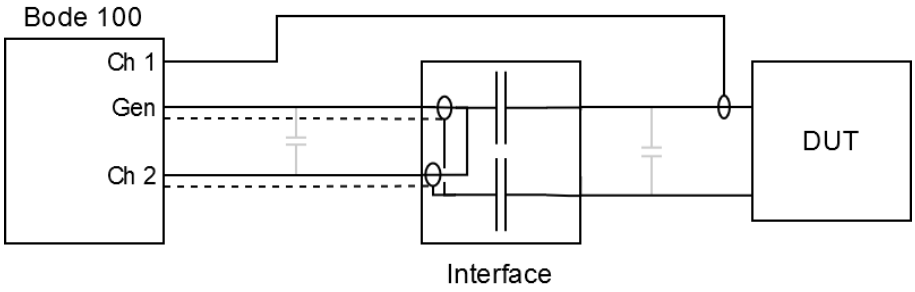

Figure 5.13: Voltage-current setup.

The faded capacitor symbols in Figure 5.13 represent parasitic parallel capacitance in the circuit. The figure emphasizes how the external current probe can achieve a more accurate current measurement by measuring close to the DUT.

5.3.3.4 Cell Type Comparison

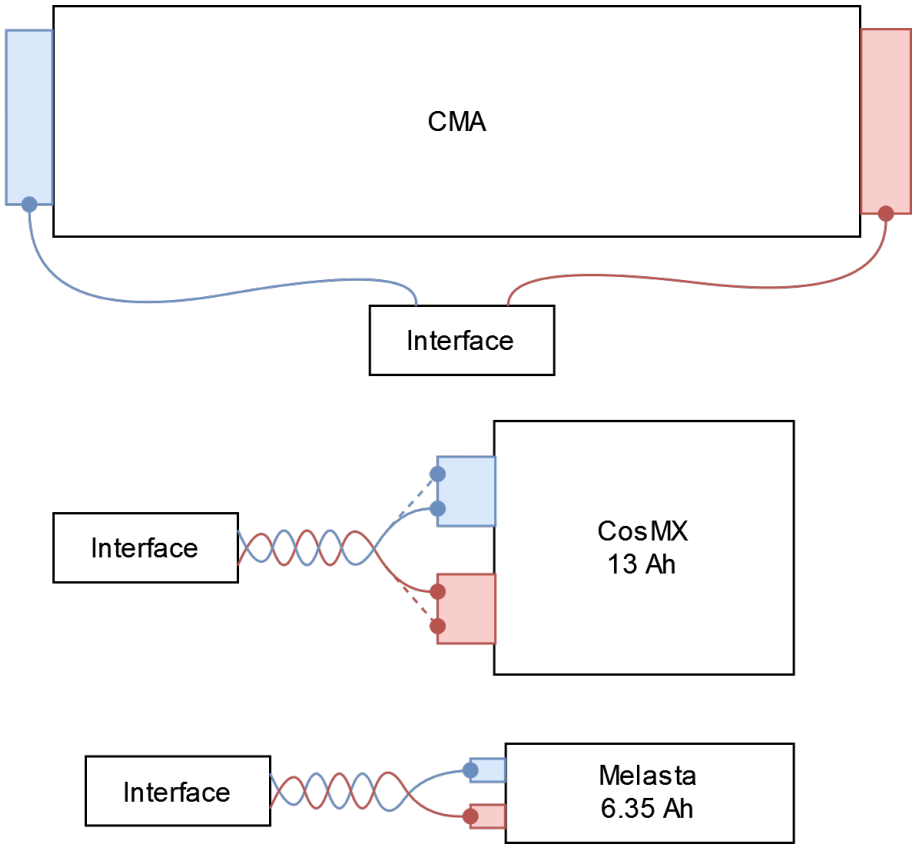

Figure 5.14: Setups for different cell types. Cell geometrical proportions are shown.

Apart from the VCC CMA cells measured in the VCC battery lab, two additional pouch cells with different geometries and chemistries were measured at Chalmers. The first is a CosMX 95B0D0HD 13 Ah NCM523 cell. The second is a Melasta SLPB9544124 6350 mAh LCO cell. The CMA cell had been in storage for $>$ 2 years and was cycled before measurement. The Melasta cell had also been in storage for $>$ 2 years, but was untouched from factory. The CosMX cell was $\approx$ 6 months old and untouched from factory.

The cells are similar in thickness. The volume and area of the cells are approximately proportional to their capacity. The CMA cell is approximately twice as large as the CosMX cell, which in turn is approximately twice as large as the Melasta cell. While both tabs of the Melasta and CosMX cells are located on the same cell side, the two tabs of the CMA cell are located on opposing sides.

The smaller cells were hypothesized to have a smaller setup inductance due to the reduced loop area (see Section 2.1.3.1) which can be seen in Figure 5.14. This is due to both the smaller size, and the placement of the cell tabs on the same side. The CosMX cell was measured twice with the crocodile clips first being placed on the inner part of the cell tabs, and later on the outer part (see Figure 5.14). This

was done to see the difference in inductance.

6

Results and Analysis

This section contains the results achieved from LTSpice circuit modelling, measurements on passive DUTs without voltage applied, measurements with a low voltage interface on single cells.

6.1 Modelling

This section shows the simulation results of the interface and VNA LtSpice model described in section 4.2 and Figure 4.8.

"Total impedance" refers to the combined impedance of the DUT, any interface(s) and any interconnections; i.e. the impedance as seen on the measurement instrument ports before any deembedding.

Figure 6.1a shows the results of using 10 different DC blocking capacitance values. We see that the low-frequency impedance increases as the capacitance of the DC-blockinc capacitors decreases. We can also see how the frequency and Q-factor of the resonance between the DC-blocking capacitors and the inductive DUT changes.

Figure 6.1b shows results from using three different configurations of the virtual DUT battery. The XsYp nomenclature refers to a battery configuration where X battery cells are connected in series, and Y series strings are connected in parallel. The three configurations thus have different DUT impedances (although only the DUT inductance is distinguishable in the results).

We see in Figure 6.1b that the total impedance at higher frequencies increases with an increase in DUT impedance. We also see that the total impedance at lower frequencies changes very little, due to the impedance in this region being dominated by the DC-blocking capacitor impedance.

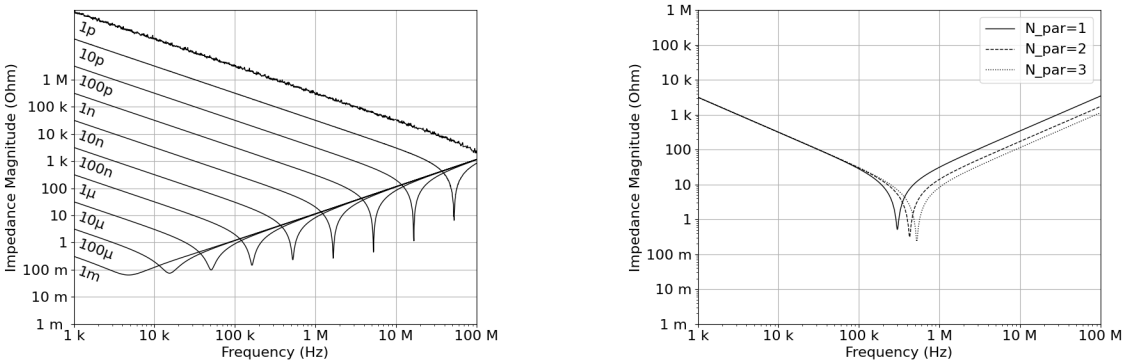

(a) Total impedance for the test setup for different DC blocking capacitance.

(b) Total impedance with 104s1p, 104s2p and 104s3p configurations.

Figure 6.1: The total impedance's dependence on DC blocking capacitance and DUT impedance. Results from simulation.

From figure 6.1b it is clear that the impedance of the DC blocking capacitors dominates at lower frequencies potentially making DUT impedance measurement difficult.

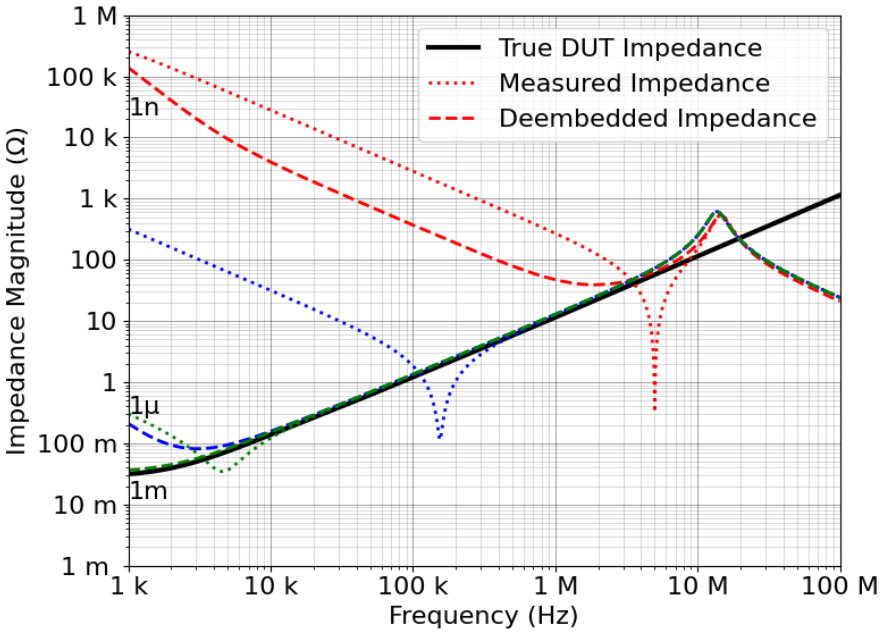

Figure 6.2: Deembedded DUT impedance compared with measured, non-de-embedded impedance and true DUT impedance.

When Equation (4.3) is applied to the simulation results, the de-embedded impedance in Figure 6.2 is obtained. It is clear that the de-embedding of the DC blocking capacitors shifts the lower bound of the valid frequency range further down by 2 orders of magnitude. It is however not possible to completely eliminate the effects of the

DC-blocking capacitors for lower frequencies where $|Z_{\mathrm{DUT}}| \ll |Z_{\mathrm{block}}|$ leads to a lack of signal. $|Z_{\mathrm{block}}|$ refers to the impedance magnitude of the DC-blocking filter for the given frequency. For more on de-embedding, see Section 2.1.6.

6.2 Measurements on passive DUTs

The results presented in this section were collected using passive components as DUTs, without any DC voltage present. The purpose is to compare the results obtained when using each interface with reference results obtained using no interface. This way, the effects of the interface can be evaluated. For DC-biased DUTs an interface will always be required making direct comparison difficult.

Measurements were conducted with the capacitive and transformer interface prototypes, as well as with the low-voltage interface.

6.2.1 Transformer based prototype

This section contains the results of measurements conducted on the transformer-based prototypes presented in Section 3.4. As previously stated, these also require some type of DC blocking component, e.g. a capacitor.

6.2.1.1 Transformer Type Comparison

The open-circuit and short-circuit impedances of the two transformers were measured. The results are presented in Figure 5.1 where it is compared with the cell impedance data presented in Section 4.1.1.

As single cell data only exists up to 100 kHz, the data is extrapolated up to 50 MHz. This is only correct if the cell has a constant inductance at higher frequencies. It is known however, that there will be parallel capacitive paths that will ”bypass” this inductance at higher frequencies; for example, the conductor-conductor capacitance. The extrapolated data is used regardless for verification purposes.

The results are also compared to an approximation of the full battery impedance extrapolated from the same single cell data. The single cell data is simply scaled with $\frac{N_{\mathrm{S}}}{N_{\mathrm{P}}}$ where N_{S} is the number of cells connected in series, and N_{P} is the number of cells connected in parallel.

Similarly to the single cell impedance, this scaling assumes the model fitted to < 100 kHz, is valid up to 50 MHz; which it, in practice, is not. The model is especially incorrect for the full battery pack, where components and geometry result in a much more complex network of parasitic capacitances and inductances.

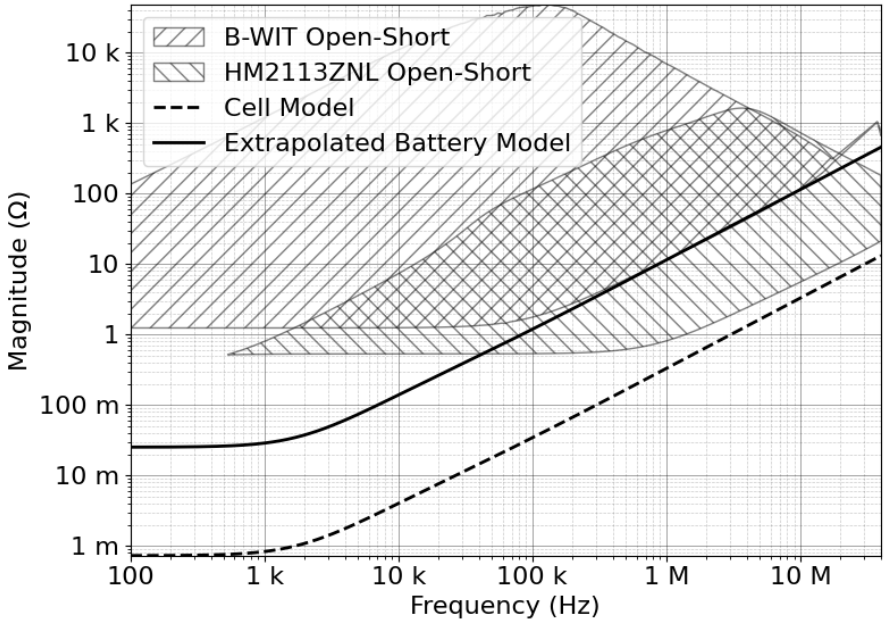

Figure 6.3: HM2113ZNL and B-WIT transformer impedance domain comparison.

In figure 6.3, the ”impedance domains” of the two prototype transformer interfaces in figure 5.1 are shown as two hatched areas. On the domain border, the DUT-to-interface impedance contrast is 1:1, i.e. $-6\,\mathrm{dB}$. Inside, the contrast increases with distance to the domain border; while outside the border, accuracy decreases with distance.

The Bode 100 receivers have a dynamic range (i.e. ratio of the largest measurable impedance to the smallest measurable impedance) of $> 100\,\mathrm{dB}$ [22] which limits how far outside the domain the instrument is able to differentiate between measurement and noise; i.e. DUT impedance and parasitic impedance. Outside this range, numerical methods like de-embedding are ineffective.

The conclusion is that measurements outside the impedance domain shown in Figure 6.3 is possible at the cost of measurement accuracy as long as the DUT-parasitic impedance ratio is sufficiently high.

The upper bound of these domain areas are constructed from the open-circuit impedance of the measurement setup as seen on the instrument port. The lower bound is constructed from the short-circuit impedance of the measurement setup as seen on the instrument port.

Also shown in figure 6.3 are the impedance plots of the single cell model (see Section 4.1), as well as the full battery model, linearly extrapolated from the same. This is to gather an understanding of whether the single cell and full battery will be measurable with respect to the interface impedance domains.

From the results in figure 6.3, it can be seen that the HM2117ZNL signal transformer shows promise for full battery pack measurements at least from 50 kHz to 20 MHz. The extrapolated battery pack impedance is in the middle of the transformer's short and open circuit impedance curves. It is possible that the single cell impedance can be measured as well above 1 MHz. Note that the single-port method is affected by series resistance and the minimum recommended impedance is 500 mΩ. Other methods would be preferred for lower impedances.

The B-WIT injection transformer has too high short-circuit resistance and inductance for the single cell measurement, and has too low isolation voltage for the full pack. Thus its use is ruled out.

6.2.1.2 DC Blocking Capacitance Comparison

The transformer prototype interface open-circuit and short-circuit impedance was measured using two different DC blocking capacitors (see Figure 3.6). These capacitors are the 2200 μF electrolytic capacitor and the 4.7 μF polyester capacitor in Table 5.1. The results can be seen in Figure 6.4.

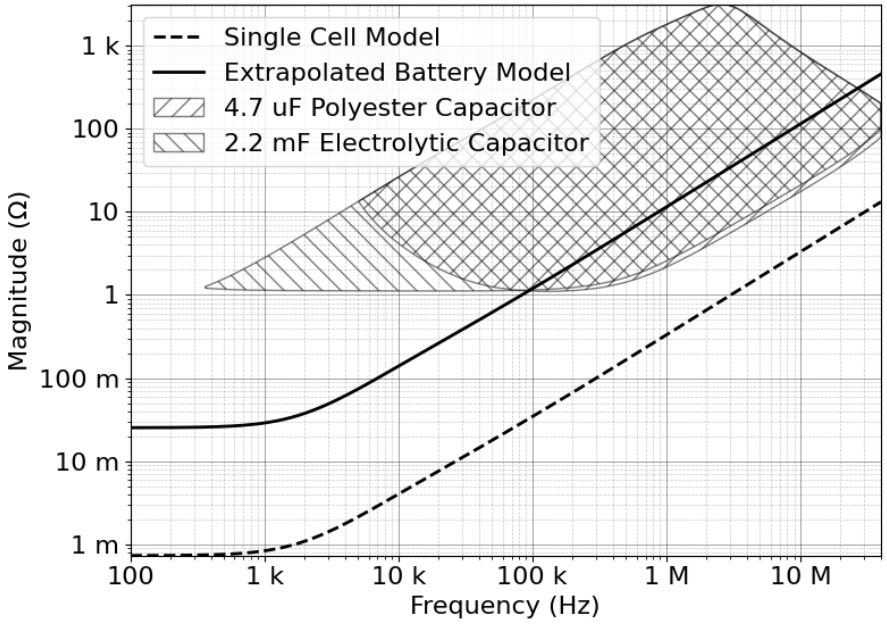

Figure 6.4: HM2117ZNL open-circuit and short-circuit impedance domain for two different DC blocking capacitances.

In Figure 6.4, it can be seen that the electrolytic capacitor has a lower low-frequency impedance compared to the polyester capacitor and is not the dominant short-circuit impedance in the 300 Hz − 100 kHz range; i.e other parasitic impedances are larger in this range. The polyester capacitor however dominates the short-circuit impedance in this range and thus affects the measurable impedance range negatively.

6.2.1.3 Measurement Results

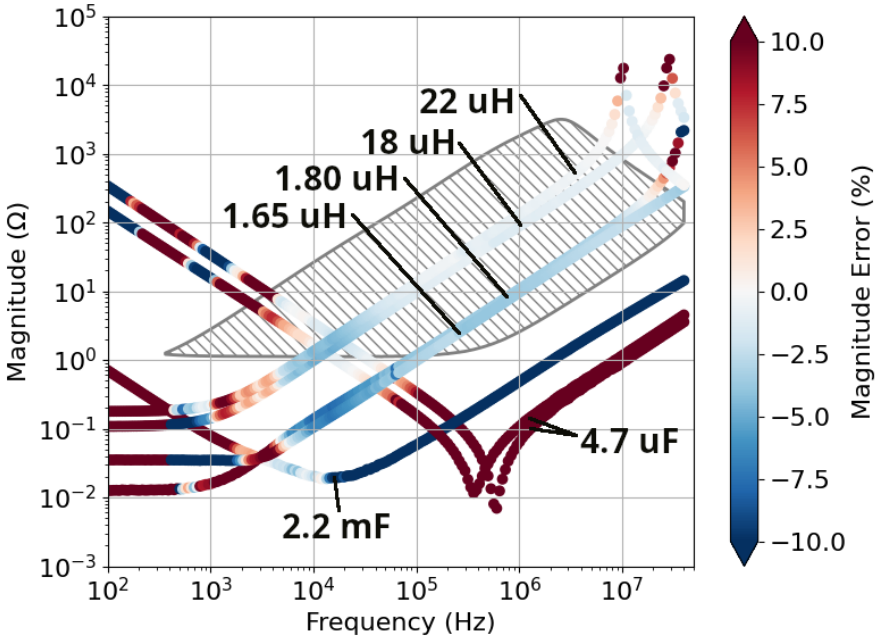

Figure 6.5: HM2113ZNL measurement errors for different inductor and capacitor measurements.

In Figure 5.4, the impedances of different inductors and capacitors measured using the Bode 100 are seen. The different DUTs are summarized in Table 5.1. No interface was connected during these measurements.

The measurements act as reference measurements to validate how well, in terms of frequency and impedance, the Bode 100 is able to reproduce the same results through the different interfaces.

The DUT components, shown in Figure 5.4, were then measured through the HM2113ZNL interface (Figure 5.1) with a 2200 μF DC-blocking capacitor.

In Figure 6.5, the reference impedance measurements of the different DUTs are shown. The data points are colored by the percentual magnitude error of the interface measurement impedance compared to the reference measurement impedance; i.e.

$$\text{Magnitude Error} = \frac{\left|Z_{\text{DUT, w/ interface}}\right|}{\left|Z_{\text{DUT,no interface}}\right|} \tag{6.1}$$

As seen in Figure 6.5, the impedances of the capacitive DUTs is lower than the interface short-circuit impedance in much of the frequency range. The error compared to the reference measurement is therefore high. Only in a very narrow frequency band is the measurement accurate. The ability to measure capacitive DUTs is important

in order to measure capacitive parasitics in the full battery.

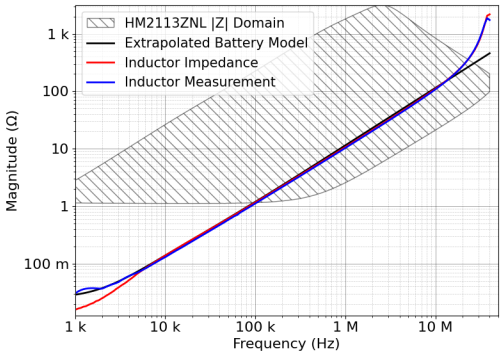

(a) Impedance magnitude.

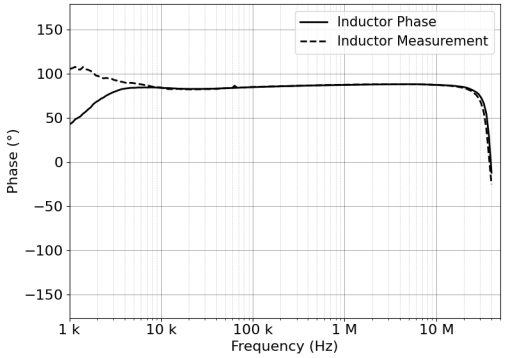

(b) Impedance phase.

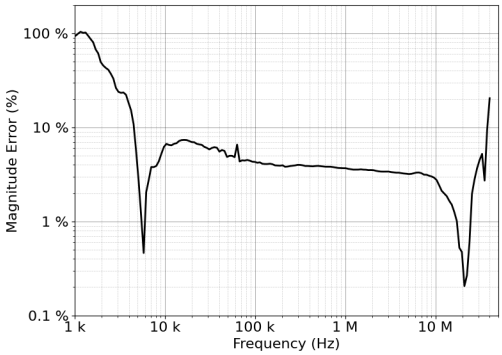

(c) Impedance magnitude error compared to measurement without interface.

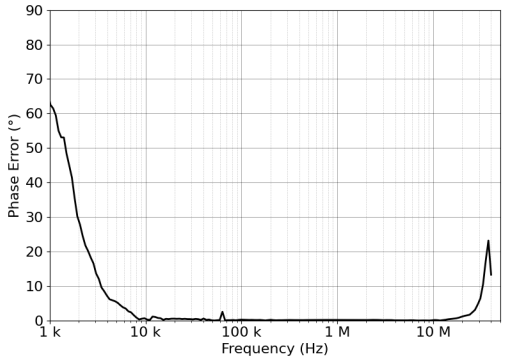

(d) Impedance phase difference compared to measurement without interface.

Figure 6.6: Results for the 1.6 μH inductor measured via the HM2113ZNL transformer and a 2200 μF DC-blocking capacitor.

The data presented in Figure 6.6 is based on the same measurements of the 1.65 μH inductor seen in Figure 6.5. The figure shows the accuracy of the measurement in more detail. This inductor was chosen to mimic the impedance of the full battery. The results show good accuracy in the 10 kHz – 10 MHz range. This range coincides with the range reported by Mazzola et al.[19][20].

Note the spurious peak at 63 kHz in Figures 6.6c and 6.6d. This peak is assumed to be inherent in the Bode 100 or its power supply as the 63 kHz sample differs to some degree in almost all conducted measurements; regardless of the measurement type, setup or DUT.

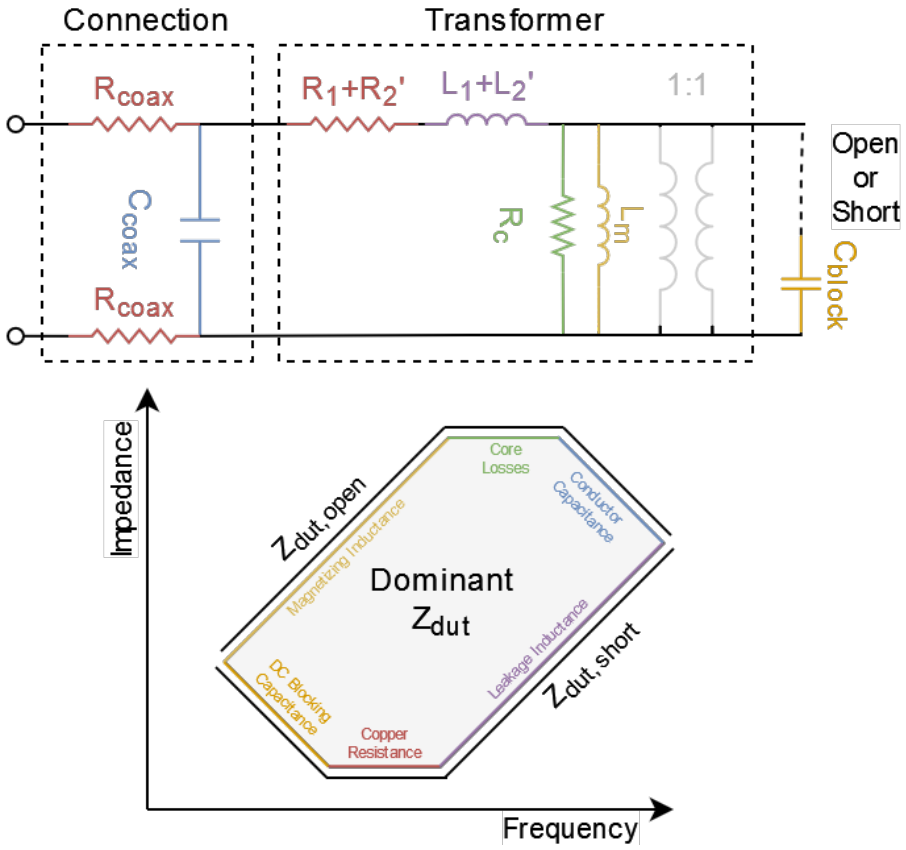

Figure 6.7:
Top: Equivalent circuit of the transformer interface showing the main parasitic elements.
Bottom: conceptual graph of open-circuit and short-circuit impedance and main parasitic elements.

Figure 6.7 shows the main parasitic elements present in the DC-blocking interface itself and how they impact the measurable impedance-frequency area.

When the output of the interface is shorted, the series impedances inherent in the setup can be measured. Lower DUT impedances can still be measured by the use of deembedding; however, accuracy will gradually diminish as the setup impedance "shadows" the DUT impedance.

For the short-circuit case, the DC blocking capacitance, parasitic series resistance, and series leakage inductance are problematic elements in their respective frequency range.

When the output poles are left open, the parallel impedances inherent in the setup can be measured. Higher DUT impedances can still be measured by the use of deembedding; however, accuracy will gradually diminish as the setup impedance "bypasses" the DUT impedance.

For the open-circuit case, the transformer magnetizing inductance, transformer core

losses, and conductor capacitance are problematic elements in their respective frequency range.

Note that any additional circuit elements (such as protection diodes, relays or bleeder resistors) will either reduce the open-circuit impedance, or increase the short-circuit impedance, leading to loss in measurement performance.

The transformer winding ratio of $N_1 : N_2$ leads to a transformation of the impedance on the secondary side to the primary side according to

$$\bar{Z}' = \left(\frac{N_1}{N_2}\right)^2 \left(\bar{Z}_{\mathrm{DUT}} + \bar{Z}_{\mathrm{cap}}\right) \tag{6.2}$$

where $\bar{Z}_{\mathrm{cap}}$ is the impedance of the DC-blocking capacitor.

According to (6.2), the transformer provides the ability to scale the secondary-side impedances in relation to the measurement instrument limits and primary-side impedances. This can prove useful if the DUT impedance is very large or very small. However, increasing the amount of transformer windings is likely to increase parasitic inductance and capacitance.

6.2.2 Capacitor based interface prototype

This section contains the results of measurements conducted on the capacitor-based prototype presented in Section 5.3.1.

6.2.2.1 Comparison of lead separation

The open-circuit and short-circuit impedances of three different test setups using the capacitor based interface were measured. The setup variation lies in the connection between the measurement instrument and the interface. In the ”direct” configuration the interface was connected to the signal generator port of the instrument by the use of a male-to-male BNC coupling. In the ”coaxial” configuration, the interface was connected to the instrument through a 0.5 m coaxial cable as in Figure 5.3a. In the banana cable setup, the connection was instead made by the use of banana leads and banana-to-BNC adapters as in Figure 5.3b.

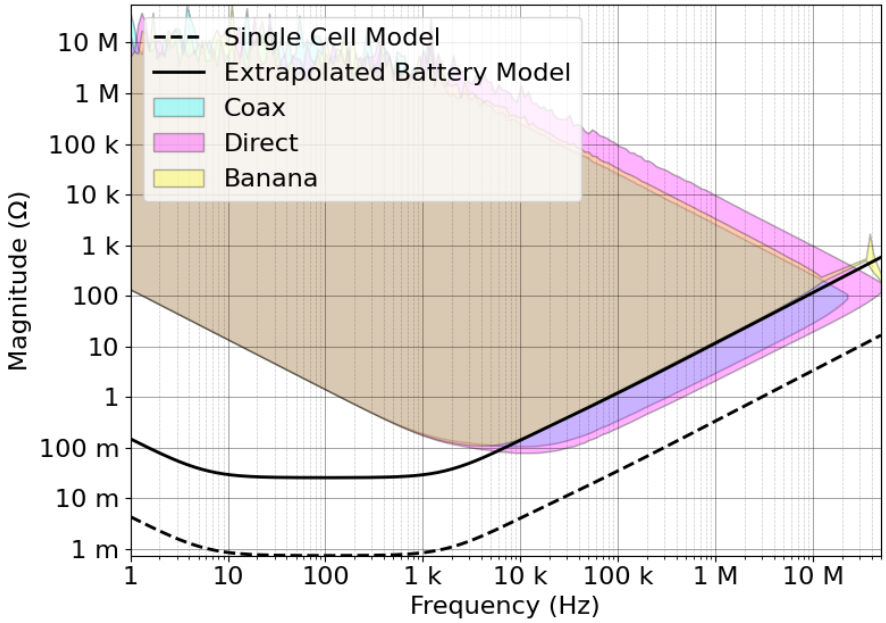

Figure 6.8: Open-circuit and short-circuit impedances measured using the capacitor-based interface prototype and three different connection types between instrument and interface.

Connection	C_{open} (pF)	L_{short} (nH)
Direct	20	340
Coax	60	480
Banana	50	2000

Table 6.1: Main parasitic components at high frequency for the three different connection types.

The resulting open-circuit and short-circuit domains can be compared in figure 6.8 and the measured values of the main parasitic components at high frequencies are presented in Table 6.1. These values are important as they affect how high in frequency the full battery (approximated with the extrapolated battery impedance seen in Figure 6.8) will be accurately measurable.

For the purpose of measuring impedance, coaxial cables are usually preferred over parallel wires. As seen in Figure 6.8 and Table 6.1 the coaxial cable exhibits a larger parasitic conductor-to-shield capacitance of $\approx 120\,\text{pF/m}$. In the banana lead case, where the conductors are further separated, this capacitance is reduced to $\approx 100\,\text{pF/m}$.

As expected, the separation of the conductors also increases the leakage inductance from $\approx 1\,\mu\text{H/m}$ to $\approx 4\,\mu\text{H/m}$. Using banana leads in the measurement circuit is therefore not recommended. This exemplifies the trade-off between the setups' in-

ductive and capacitive limits.

6.2.2.2 Measurements on passive DUTs

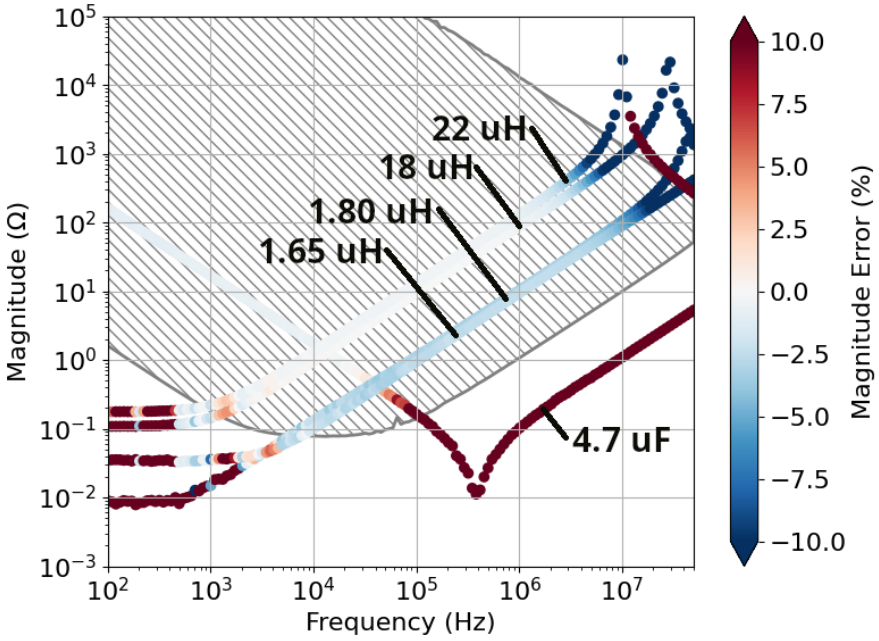

Figure 6.9: Impedance versus frequency for different DUTs measured with and without capacitive interface.

The same measurements conducted in Section 6.2.1.3 were conducted using the capacitor-based interface prototype. The results for the different DUTs can be seen in Figure 6.9. The figure shows the measurement error added by the capacitor based interface.

Comparing Figure 6.9 with the results in figure 6.5, the magnetizing inductance of the transformer no longer limits the upper impedance limit in the lower frequency region of the 4.7 μF MLCC capacitor measurement. Note the absence of the transformer magnetizing inductance and cores losses Figure 6.7 when compared to Figure 6.11.

From Figure 6.9, it is clear that low-frequency measurements of the 1.65 μH inductor (that emulates the full battery) would benefit from an even higher DC blocking capacitance and an even lower interface ESR. At high frequencies the parasitic capacitance between the measuring conductors is a limiting factor.

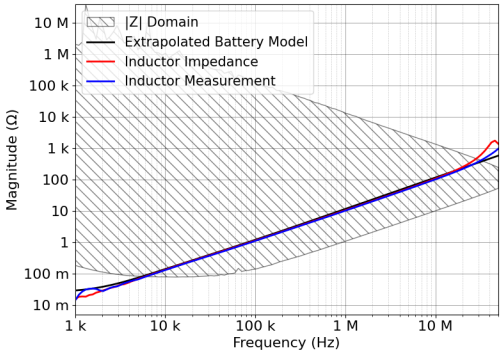

(a) Impedance magnitude.

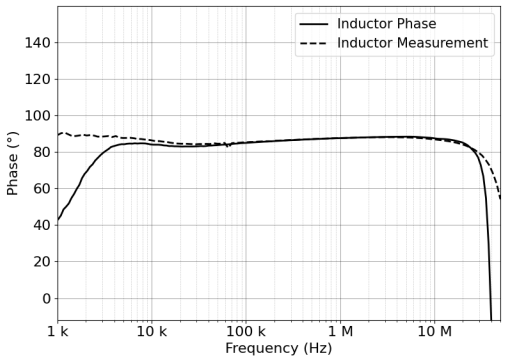

(b) Impedance phase.

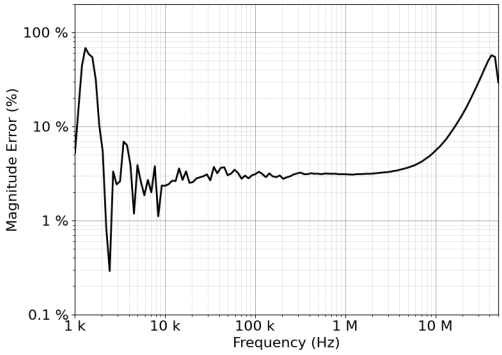

(c) Impedance magnitude error compared to measurement without interface.

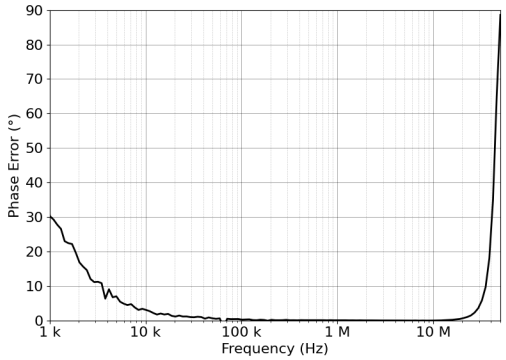

(d) Impedance phase error compared to measurement without interface.

Figure 6.10: Measured impedance versus frequency for the 1.6 μH inductor measured via the capacitor-based interface prototype.

Figure 6.10 shows the measurement difference between measurements of the inductor representing the inductance of a full battery pack (#1 in Table 5.1 and Figure 5.4), with and without the capacitor based interface. These results can be compared to the results for the transformer based interface seen in Figure 6.6.

The results in Figure 6.10 show a satisfactory accuracy both in impedance magnitude and phase. In the frequency range from 10 kHz to 10 MHz, the magnitude error is $< 5\,\%$ and the phase error is $< 5\,^{\circ}$.

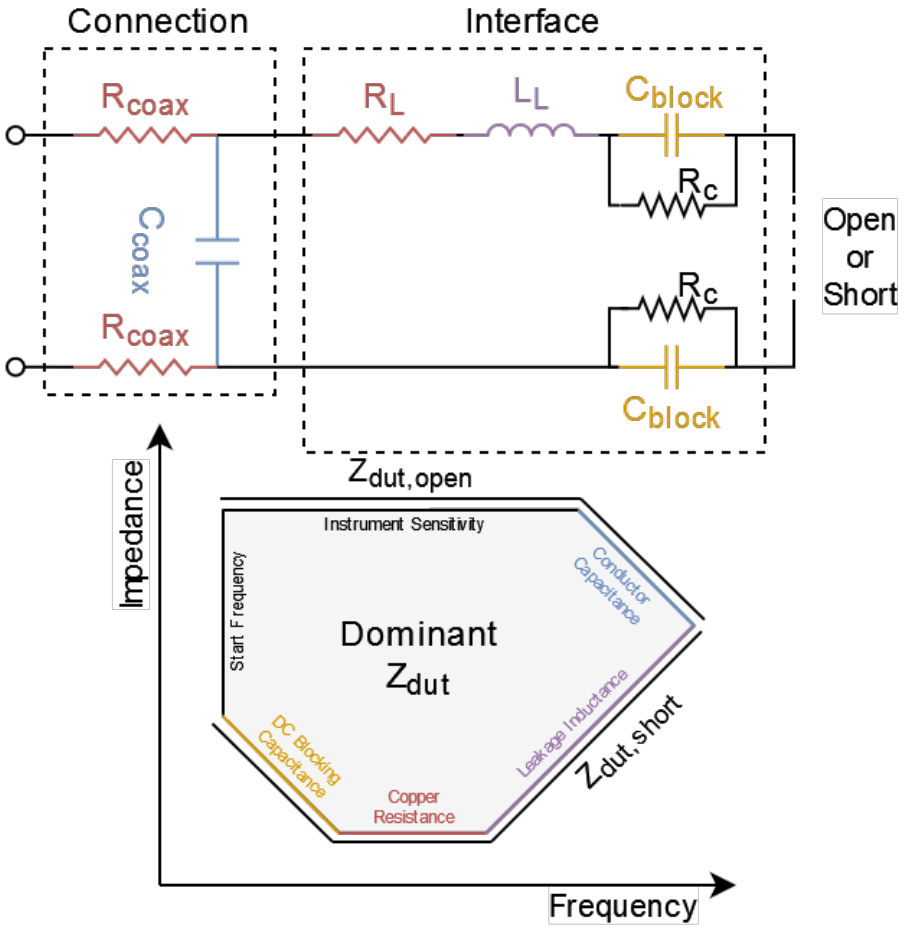

Figure 6.11: Top: Equivalent circuit of a capacitor-based interface showing the main parasitic elements.
Bottom: conceptual graph of open-circuit and short-circuit impedance and main parasitic elements.

Figure 6.11 shows the main parasitic elements present in the interface itself as well as their impact on impedance measurability.

When the output of the interface is short-circuited, the series impedances inherent in the setup can be measured. Lower DUT impedances can still be measured by the use of deembedding; however, accuracy will gradually diminish as the setup impedance "shadows" the DUT impedance.

For the short-circuit case, the DC blocking capacitance, parasitic series resistance, and series leakage inductance limit the lowest measurable impedance at low, medium and high frequencies respectively; see Figure 6.11.

When the output poles are left open, the parallel impedances inherent in the setup can be measured. Higher DUT impedances can still be measured by the use of deembedding; however, accuracy will gradually diminish as the setup impedance "bypasses" the DUT impedance.

For the open-circuit case, the instrument sensitivity and conductor capacitance limit the highest measurable impedance at low to medium and high frequencies, respectively.

Note that compared to the transformer-based interface, see Section 3.4 and Figure 6.7, there is no longer any magnetizing inductance present that would otherwise limit the higher impedance limit at lower frequencies.

6.2.3 Measurement Interface for Few Cells

The results in this section come from measurements conducted with the low voltage interface presented in section 5.3.1.

6.2.3.1 Effects of Multimeter Voltage Monitoring

For battery pack testing, a request from the battery lab personnel was the ability to monitor the pack voltage during the measurement process. This would entail connecting a voltmeter across the DUT poles. Measurements were conducted in order to quantify how the voltmeter would affect the measurements.

In Figure 6.12 the open-circuit and short-circuit impedances of the measurement setup with and without a voltmeter is seen.

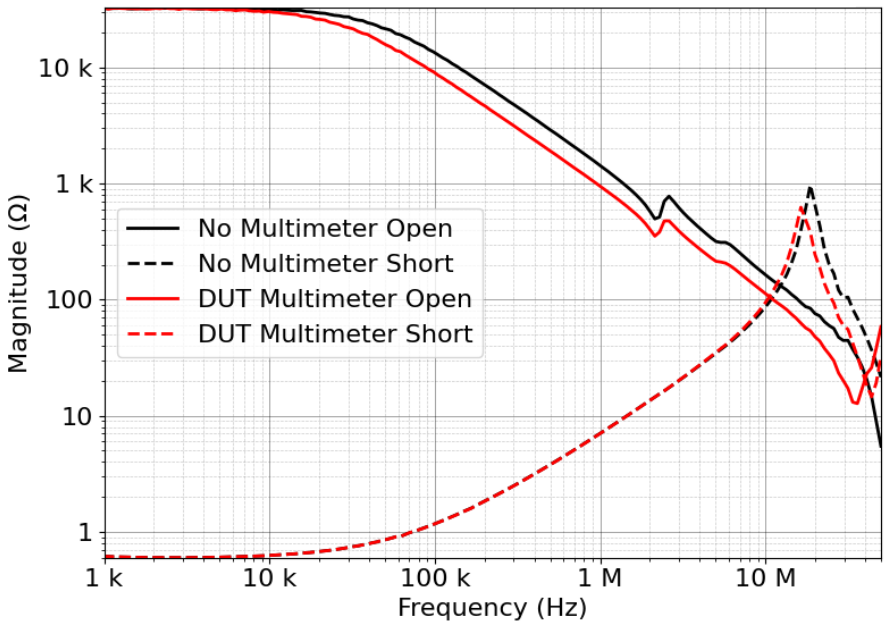

Figure 6.12: Open-circuit and short-circuit impedances with and without multimeter connected.

As seen in Figure 6.12, inserting a multimeter into the measurement circuit will load the measurement with parallel capacitance in the order of tens of picofarads.

The exact amount depends on the instrument. This capacitive loading is likely to cause issues when the DUT capacitance to be measured is close to or lower than this parasitic capacitance. It is preferable to avoid loading the circuit with monitoring equipment as long as safe operation can be proven.

6.2.3.2 EMI shielding comparison

Measurements of the open- and short-circuit interface impedances were conducted with the chamber door opened and closed respectively. The result can be seen in Figure 6.13.

The purpose of the measurements was to identify any measurement errors caused by external electrical noise and ways of preventing them from from affecting other measurements. The hypothesis was that accurate measurement required the setup to be shielded from external electrical noise.

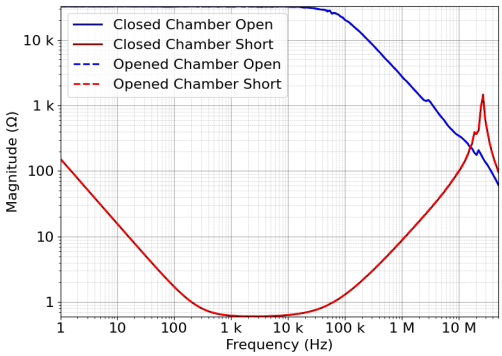

(a) Open-circuit and short-circuit impedances with chamber open and with chamber closed.

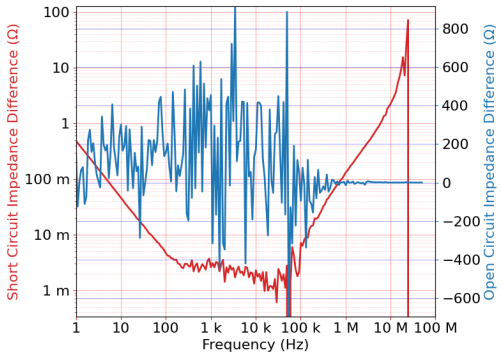

(b) Impedance difference between opened and closed chamber measurements.

Figure 6.13: Measured impedance versus frequency for open and closed chamber measurements

No significant change in the measurement results (Figure 6.13a) were noticed when the door to the chamber was left opened as compared to when the chamber is completely electrically shielded.

In Figure 6.13b the short circuit impedance difference has defined features. Measuring the increasing slope an difference in series inductance of 20 nH can be calculated. This change can possibly be attributed to a larger air volume leading to increased leakage inductance. However, the same measurements also indicate an increase in series capacitance and resistance, which is harder to justify. The likely explanation is that the error only is proportional to the measured impedance.

For the open circuit measurement, no well-defined features could be observed. Note that the short-circuit impedance difference graph uses logarithmic scaling, while the open-circuit impedance difference graph uses linear scaling. The leakage resistance

and parallel capacitance that determine the open circuit impedance is not expected to differ in the two cases.

No spurious noise was noticed in the measurement results. The Volvo battery lab is expected to be quite noisy as it contains a lot of high power electrical equipment such as compressors, climate control systems, chargers and electrical loads in constant operation. However, this did not affect the measurement results.

Measurements conducted in the office with the unshielded interface prototypes (Figures 5.1 and 5.3) usually contained a spurious impedance magnitude peak and phase disturbance at $\approx 63\,\text{kHz}$. The same distortions seem to be present also for the tests conducted with the shielded interface in the shielded test chamber (see for example Figures 6.14 and 6.18). The Bode 100 itself and its power supply are the only noise sources common to these measurements.

6.3 Cell measurements

The results presented in this section were collected from cell measurements conducted in the jig seen in Figure 5.12 with the capacitor-based interface presented in Section 5.3.1. The different measured cells can be seen in Figure 5.14.

6.3.1 One-port and two-port comparison

Measurements were conducted on CMA cells with the same setup, first with the one-port reflection method (Section 3.3.3), and after that with the two-port shunt-thru method (Section 3.3.1). The results of the two are compared in Figure 6.14.

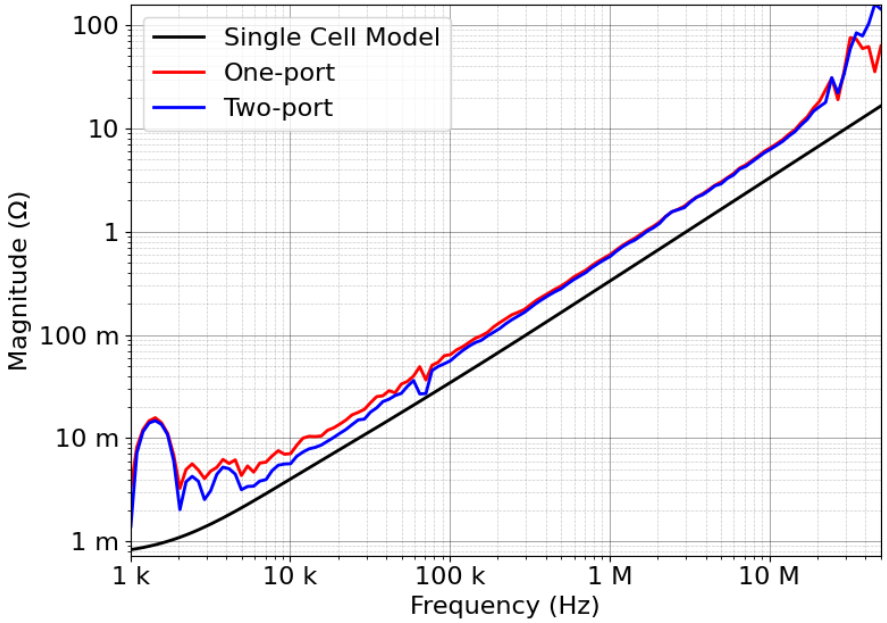

Figure 6.14: Impedance versus frequency of a single CMA cell measured with the interface using the one port and two port method respectively.

From Figure 6.14 it appears that the two-port method succeeds in reducing the effects of the coaxial cables' DC resistance, if only slightly. This is seen from the reduction in measured impedance at lower frequencies, where the DC resistance of the setup is expected to dominate.

The measurement results do not converge with the reference model that is based on EIS-data. They indicate an inductance twice as large as expected. This indicates that the parasitic setup inductance is too large compared to the cell inductance for the Bode 100 to de-embed completely.

The parasitic inductance can be reduced by reducing the conductor length between DUT and receiver (Bode 100 input channel or differential amplifier). In these tests, no further reduction of length was possible without increasing the interface complexity and design effort. The interface circuit board itself contained slight design errors and can be improved marginally by re-routing traces for reduced inductance.

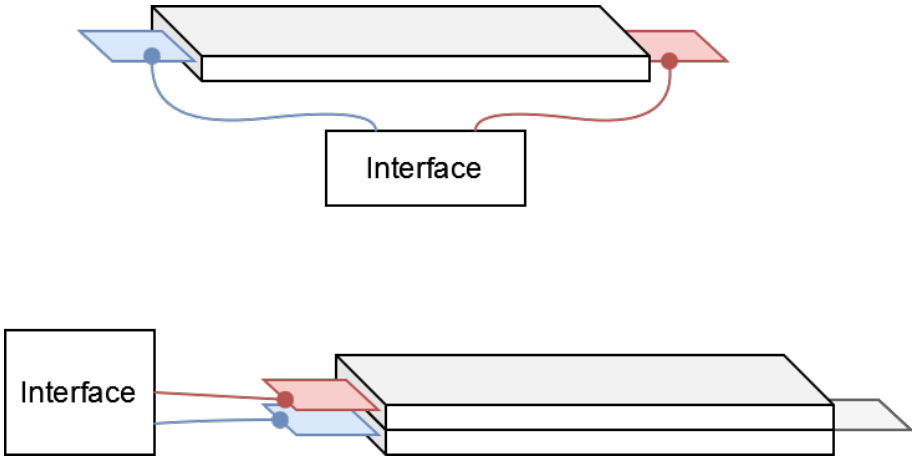

Figure 6.15: Diagram of the used single cell setup and the proposed two-cell setup.

One way to reduce the parasitic inductance is to measure two series connected cells instead of a single cell as seen in Figure 6.15. An issue in the previous measurement is the fact that the cell poles are on opposite ends of the 35 cm long cell. This means the DUT connecting leads form a large loop area increasing the setup inductance. By letting the second cell form the return path from the far pole, the connecting cables can be kept short and twisted, reducing the setup impedance. The series connection also means the DUT impedance is doubled, providing yet higher contrast between the DUT impedances and parasitic impedances. The closest electrodes of the two cells would however be capacitively coupled, affecting results at higher frequencies.

6.3.1.1 Coaxial shield grounding comparison

Measurements on CMA cells were conducted with the shields of the coaxial connectors shorted, by the use of conductive tape, to the aluminum enclosure which is grounded to the protective earth of the interface's 24 V power supply. The results are seen in Figure 6.16. Note that the Bode 100 uses an isolated power supply without protective earth, i.e. there is no protective earth connecting the Bode 100 signal input and the power supply.

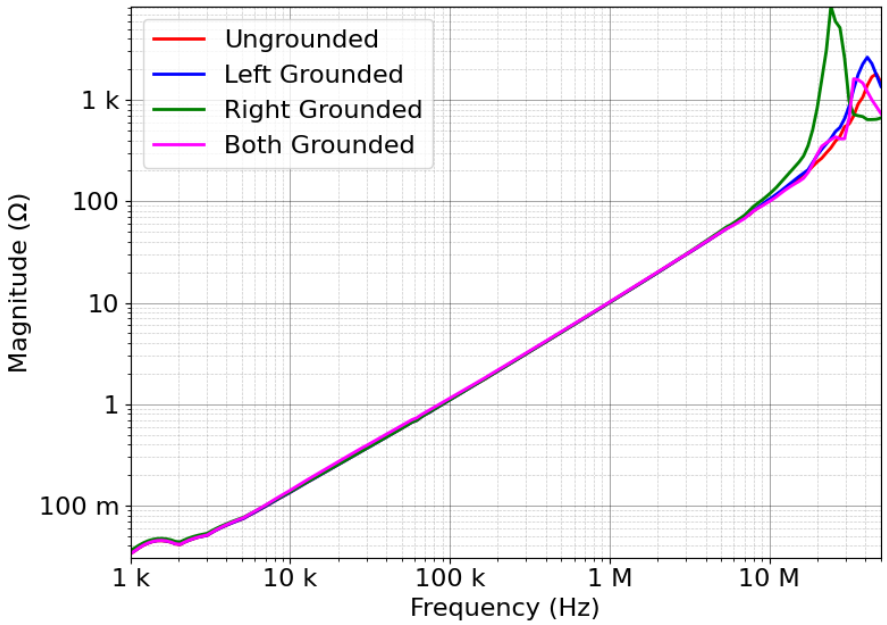

Figure 6.16: Measurements of cell impedance with the two BNC connectors grounded or isolated in different combinations.

No significant differences can be seen in the measurmeent results in the 10 kHz to 5 MHz range. This is in conflict with the large differences presented by Doersam et al. in [3]. No concusion is drawn about the cause of the differences at frequencies above 5 MHz.

6.3.2 Current clamp comparison

Voltage-current measurements were conducted using two different high frequency current clamps, see Section 5.3.3.3. The results are compared with the expected impedance and two-port measurements in Figure 6.17.

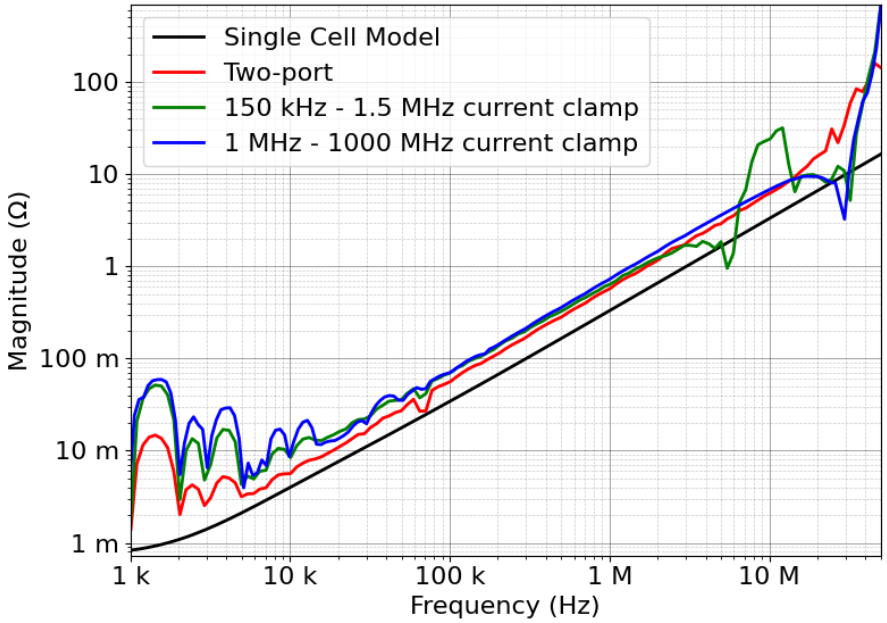

Figure 6.17: Cell impedance versus frequency measured using two setups with different current clamps and one without.

The current clamps were intended to improve the measurement accuracy by bypassing the current loading from the parallel capacitance in the setup (see Figure 5.13 and conductor capacitance in Figure 6.11). The current clamp methods saw no improvement due to the methods being limited by the large series inductance compared to the DUT impedance. For the full battery pack, the use of a current clamp may be useful depending on its impedance characteristics.

6.3.3 Temperature comparison

A two-port shunt-thru measurement (see section 3.3.1) was conducted on the CMA cells at 22.4 °C and 35 °C. The results can be seen in Figure 6.18

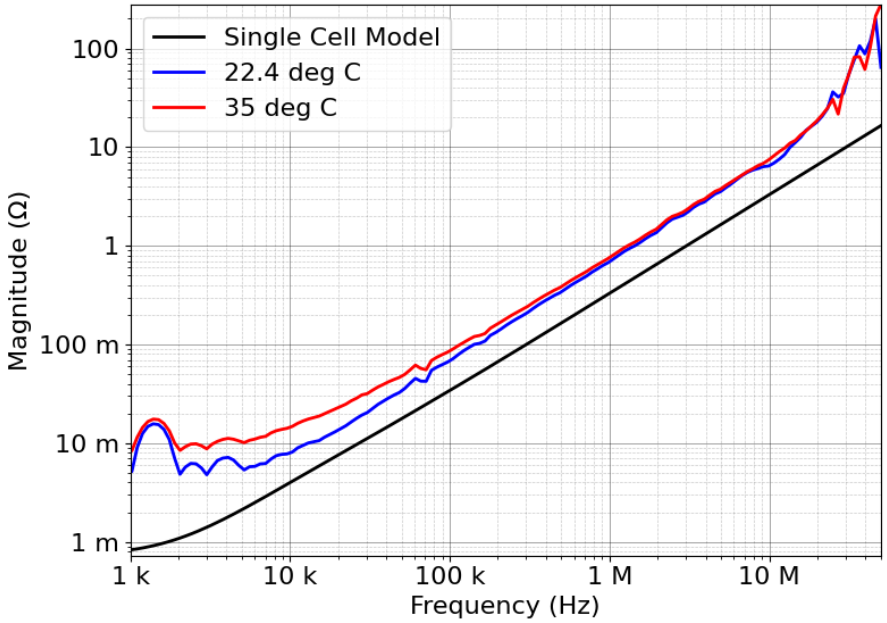

Figure 6.18: Cell impedance versus frequency with cells acclimatized to 22.4 °C and 35 °C respectively.

Note that the measurement was conducted with the whole setup, including the Bode 100, placed inside the chamber; meaning it also could be affected by the temperature difference. The Bode 100 is however rated to 40 °C in operation and calibration was conducted after the temperature was reached in order to minimize the effect.

The increased low frequency impedance of the 35 °C cell in Figure 6.18 is probably due to an increase in the DC resistance of the cell and/or setup. Similarities can be seen with the difference between one-port and two-port measurements presented in Figure 6.14, where the two-port measurement aims to reduce the effects of series resistance.

6.3.4 DUT cable thickness comparison

Both 0.22 mm^2 and 4 mm^2 banana cables were tested in between the interface and the DUT. The hypothesis was that the thicker cables would exhibit a reduced inductance. The results are seen in Figure 6.19.

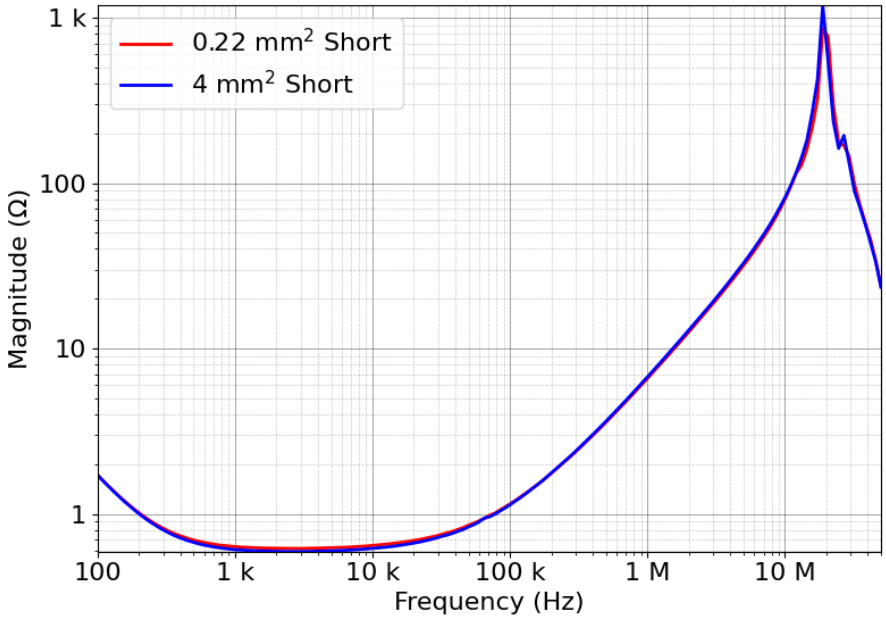

Figure 6.19: Measured short circuit impedance versus frequency of measurement interface when using cables with a cross-sectional area of $0.22\,\mathrm{mm}^2$ and $4\,\mathrm{mm}^2$ respectively.

The results in Figure 6.19 show only an insignificant difference in impedance between the two measurements. There is a reduction in series resistance by $\approx 20\,\mathrm{m\Omega}$ and an increase in series inductance by $\approx 32\,\mathrm{nH}$. The increase in inductance is hypothesized to be due to a slight change in cable loop area as the thicker cables are not as easy to route for reduced inductance.

6.3.5 Cell Type Comparison

The results of the measurements conducted on the three different cell types presented in Section 5.3.3.4 can be seen in Figure 6.20.

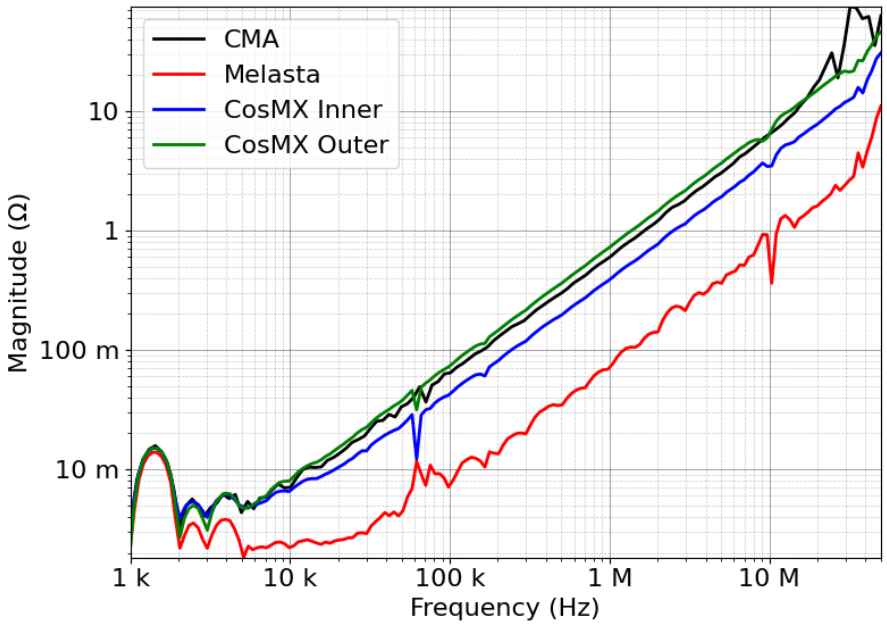

Figure 6.20: Measured impedances of three cell types of different geometries, capacities and chemistries.

The absolute values in this graph should be taken with a grain of salt as the non-CMA cell impedances are even lower than previous measurements which were proven to not be fully accurate. The Melasta cell is small and has a very low series inductance. The ”bumps” in the Melasta plot originate from the Bode 100 instrument itself when the impedance is too small for accurate measurement or deembedding.

As expected, the CosMX cell has a greater inductance; and this inductance increases when the crocodile clips are connected further apart on the cell tabs.

7
Conclusion

7.1 LV Impedance Interface

The interface presented in the thesis (see Section 5.3) has been used to measure impedances of passive components from 10 kHz to 10 MHz. It has also been operated successfully for measurements on energized lithium-ion cells. However, the parasitic series inductance and series resistance in the used interface are too large to enable accurate impedance measurements on single cells.

Similar interfaces can however be used for battery impedance measurements given that the battery impedance is greater than the short-circuit impedance of the interface.

7.2 Interface Limitations

The interface frequency range is limited due to the parasitic elements presented in Figure 6.7 and 6.11. The practical bandwidth of the interface was approximately 10 kHz to 10 MHz when used to measure the cells seen in Figure 5.14. The effect of these parasitic elements can be mitigated by the use of different measurement methods presented in chapter 3.

7.3 Impact on Sustainability

The work contributes to an improved understanding of the EMC characteristics of electric vehicle powertrains and systems in their prototype phase. This enables improved accuracy when optimizing complex electrical systems, leading to reductions in material usage. This improvement is due to expected possibilities of reducing EM filter count and size, EM shielding and other components. The resulting cost reduction also contributes to an increased adoption of EVs leading to a reduced dependence on fossil fuels.

8

Future work

8.1 Future interfaces

For future impedance measurements, the thesis conclusion is that no single interface is able to span the whole frequency range from 1 kHz to 100s of MHz. It is recommended to design interfaces with higher accuracy within a narrow bandwidth. Measurements using multiple different interfaces, which are optimized for different bandwidths, can then be combined to obtain the impedance over the full bandwidth.

8.1.1 Low Frequency Measurements

For low frequency measurements (approximately 100 Hz−10 kHz), it is recommended to implement a transformer-capacitor based interface (Figure 3.6). External amplifiers are not needed as the series inductance and parallel capacitance of the interface is no issue in this frequency range. Instead, an interface based on passive components can be used, together with a VNA. When DUT impedance and measurement frequency is low, common mode chokes or differential amplifiers may still be required in order to eliminate effects due to ground loops (see Figures 5.11 and 5.10).

It is shown in the thesis, that a transformer-capacitor solution is preferable due to a 4x decrease in DC blocking capacitor effective impedance. This is because the two series connected capacitors used in a capacitor-based interface can be connected in parallel in a transformer-based interface.

This transformer requires a fairly large magnetizing inductance to preserve accuracy at higher impedances at lower frequencies (see Figure 6.3). This magnetizing inductance requires a large transformer core volume and weight to avoid magnetic saturation at low frequencies. The inductance is recommended to be at least 200 mH as measurements with the B-WIT indicates this inductance will enable measurements of up to 100 Ω down to 100 Hz.

For the full battery model with its expected internal resistance of 20 mΩ, the DC blocking capacitance required is expected to be 4 mF for measurements down to 1 kHz and 40 mF when measuring down to 100 Hz. In order to measure such low impedances at such low frequencies, the parasitic resistance of the interface needs to be circumvented by the use of 4-wire measurements that would require two interfaces (see figs. 5.10, 6.14).

8.1.2 High Frequency Measurements

For higher frequency measurements ($\approx$ 10 MHz+) it is recommended to implement an interface similar to the one presented by Widek (Figure 3.2), where high impedance differential amplifiers measure voltage and current as close as possible to the DUT itself. The aim is to eliminate as much series inductance, parallel capacitance and signal reflection as possible.

Another recommendation is to simulate the interface in order to evaluate its inherent parasitic components and ways to reduce their effect.

The thesis makes no conclusion in favor of transformer-capacitor or capacitor-capacitor interface for the high frequency range. The selection of transformer and capacitors depends mainly on the series inductance or parallel capacitance of the components.

A large DC-blocking capacitance will hinder measurements at low impedances and low frequencies. A large Magnetizing inductance will hinder measurements at high impedances and low frequencies. Different transformers will likely present trade-offs between their parasitic impedances.

Bibliography

[1] A. Henriksson, J. Lektenius, A. Bergqvist, *et al.*, *Rifel - ripple and electromagnetic fields in electric vehicles.* 2018. [Online]. Available: https://research.chalmers.se/publication/504008.

[2] P. Widek and M. Alakula, "Modeling of electric power system in electric vehicles," English, in *2020 International Symposium on Power Electronics, Electrical Drives, Automation and Motion, SPEEDAM 2020*, ser. 2020 International Symposium on Power Electronics, Electrical Drives, Automation and Motion, SPEEDAM 2020, 2020 International Symposium on Power Electronics, Electrical Drives, Automation and Motion, SPEEDAM 2020 ; Conference date: 24-06-2020 Through 26-06-2020, United States: IEEE - Institute of Electrical and Electronics Engineers Inc., 2020, pp. 293–298. DOI: 10.1109/SPEEDAM48782.2020.9161884.

[3] T. Doersam, S. Schoerle, E. Hoene, K.-D. Lang, C. Spieker, and T. Waldmann, "High frequency impedance of li-ion batteries," in *2015 IEEE International Symposium on Electromagnetic Compatibility (EMC)*, 2015, pp. 714–719. DOI: 10.1109/ISEMC.2015.7256251.

[4] [Online]. Available: https://www.allaboutcircuits.com/tools/wire-loop-inductance-calculator/.

[5] *Warburg impedance.* [Online]. Available: https://www.palmsens.com/knowledgebase-topic/warburg-impedance/.

[6] Omicron Lab, *Application note - impedance measurements with the bode 100.* [Online]. Available: https://www.omicron-lab.com/fileadmin/assets/Bode_100/ApplicationNotes/Impedance_Measurement_methods_using_the_Bode_100/2020-10-21_Bode_Appnote_Impedance_Measurements_V1_0.pdf.

[7] *What are s-parameters?* [Online]. Available: https://www.ansys.com/simulation-topics/what-are-s-parameters.

[8] Omicron Electronics Corp., *Bode 100 application note - battery impedance measurement.* [Online]. Available: https://www.omicron-lab.com/applications/detail/news/battery-impedance-measurement#.

[9] Tektronix, *Tektronix high voltage differential probes product page.* [Online]. Available: https://www.tek.com/en/datasheet/high-voltage-differential-probes.

[10] Gamry Instruments, *Gamry reference 3000 - operators manual.* [Online]. Available: https://www.gamry.com/assets/Uploads-v2/Reference-3000-Operators-Manual-v2.pdf.

[11] Hioki E. E. Corporation, *Hioki ct16711 manual*. [Online]. Available: https://www.hioki.com/in-en/download/30550.

[12] Teledyne LeCroy, *Teledyne t3rc datasheet*. [Online]. Available: https://www.mouser.se/datasheet/2/227/TELEDYNE_T3RC_Data_Sheet_27July21-2525269.pdf.

[13] P. Widek, personal communication, Mar. 8, 2024.

[14] T. F. Landinger, G. Schwarzberger, and A. Jossen, "A novel method for high frequency battery impedance measurements," in *2019 IEEE International Symposium on Electromagnetic Compatibility, Signal & Power Integrity (EMC+SIPI)*, 2019, pp. 106–110. DOI: 10.1109/ISEMC.2019.8825315.

[15] K. Creel, *Measuring transformer distributed capacitance*. [Online]. Available: https://datatronics.com/pdf/distributed_capacitance_paper.pdf.

[16] H. Jie, Z. Zhao, F. Fei, R. Simanjorang, F. Sasongko, and K. Y. See, *A survey of impedance measurement methods in power electronics*, 2022. arXiv: 2204.06095 [physics.ins-det].

[17] Omicron Lab, *Bode 100 user manual*. [Online]. Available: https://www.omicron-lab.com/fileadmin/assets/Bode_100/Manuals/Bode-100-User-Manual-ENU10060503.pdf.

[18] Picotest Measurement Solutions, *Extended-range shunt-thru measurement*. [Online]. Available: https://youtu.be/mt6U2PXjluQ?si=8t00WCjBQYrG9DIN.

[19] E. Mazzola, A. Amaducci, E. F. Bononi, and V. Montanaro, "Measurement of lifepo4 battery modal impedances under different conditions," in *2021 Asia-Pacific International Symposium on Electromagnetic Compatibility (APEMC)*, 2021, pp. 1–4. DOI: 10.1109/APEMC49932.2021.9596734.

[20] E. Mazzola, F. Grassi, and A. Amaducci, "Novel measurement procedure for switched-mode power supply modal impedances," *IEEE Transactions on Electromagnetic Compatibility*, vol. 62, no. 4, pp. 1349–1357, 2020. DOI: 10.1109/TEMC.2019.2941449.

[21] S. Long, *Ece145a/218a course notes - #4 s-parameters*. [Online]. Available: https://web.ece.ucsb.edu/~long/ece145a/Notes4_Sparams.pdf.

[22] Picotest Measurement Solutions, *Bode 100 datasheet*. [Online]. Available: https://www.omicron-lab.com/fileadmin/assets/Bode_100/Documents/Bode_100_R2_Technical_Data_V1.3.pdf.

DEPARTMENT OF ELECTRICAL ENGINEERING
CHALMERS UNIVERSITY OF TECHNOLOGY
Gothenburg, Sweden
www.chalmers.se

CHALMERS
UNIVERSITY OF TECHNOLOGY